POLITECNICO DI MILANO
Master of Science in Computer Engineering
Dipartimento di Elettronica, Informazione e Bioingegneria

A novel cost-effective parallel narrowband ANC system with local secondary-path estimation

Supervisor: Prof. Luigi Piroddi
Co-supervisor: Prof. Giancarlo Bernasconi

Master Graduation Thesis by:
Riccardo Delegà, id. 817744

Academic Year 2014-2015

POLITECNICO DI MILANO
Laurea Magistrale in Ingegneria Informatica
Dipartimento di Elettronica, Informazione e Bioingegneria

A novel cost-effective parallel narrowband ANC system with local secondary-path estimation

Relatore: Prof. Luigi Piroddi
Correlatore: Prof. Giancarlo Bernasconi

Tesi magistrale di:
Riccardo Delegà, matricola 817744

Anno Accademico 2014-2015

Sommario

Il rumore ambientale è un problema pervasivo nella società odierna. Esposizioni per lunghi periodi di tempo a rumori acustici di forte intensità hanno ripercussioni gravi di tipo fisico, fisiologico e psicologico sulle persone. Per far fronte a questi problemi, sono state sviluppate tecniche di controllo attivo del rumore (Active Noise Control - ANC), che rimuovono efficacemente i rumori a bassa frequenza.

In questa tesi presentiamo un nuovo sistema di controllo attivo del rumore a banda stretta (Narrowband Active Noise Control - NANC) che è basato sull'identificazione di stime locali di basso ordine del cammino secondario. Il sistema proposto permette di ridurre il costo computazionale associato alle operazioni di filtraggio del segnale di riferimento nei sistemi NANC basati sull'algoritmo FxLMS, mantenendo allo stesso tempo prestazioni paragonabili in termini di cancellazione del rumore e velocità di convergenza. Inoltre, il sistema proposto offre robustezza ai cambiamenti nel cammino secondario, grazie al basso ordine delle stime locali utilizzate. Questo lavoro fornisce anche una legge empirica di correzione del guadagno dell'algoritmo adattivo, che è equivalente alla versione normalizzata dell'algoritmo FxLMS.

Il sistema proposto viene confrontato con il sistema NANC tradizionale e con due varianti efficienti dal punto di vista computazionale che sono state studiate nella letteratura. Le analisi computazionali e le simulazioni effettuate mostrano che il sistema proposto riduce notevolmente il costo computazionale del sistema NANC tradizionale senza peggiorare le prestazioni in maniera significativa. Inoltre, le simulazioni mostrano che le stime locali si adattano ai cambiamenti nel cammino secondario più rapidamente rispetto alla stima globale utilizzata finora in letteratura.

Abstract

Environmental noise is ubiquitous and pervasive in our society. Long-term exposure to high-intensity acoustic noise has severe and far-reaching physical, physiological and psychological effects on human beings. For this reason, active noise control (ANC) techniques have been developed to remove low-frequency noise.

We present in this thesis a novel narrowband ANC (NANC) system based on the identification of low-order local secondary-path estimates that reduces the computational cost associated to the reference-filtering operations of FxLMS-based NANC systems while retaining their performance characteristics. The proposed system offers more reactive secondary path online modelling thanks to the low-order of the employed secondary path estimates. We also provide a step size-correction law that acts as a normalisation term for the FxLMS algorithm.

We compare the proposed system with the traditional NANC system and two cost-effective NANC systems in the literature. Computational analyses are provided and computer simulations are carried out to assess the performance of the proposed system. The proposed system reduces the number of required computations with respect to the traditional NANC system and its online-modelling subsystem is faster in adapting to changes in the secondary path with respect to global online-modelling subsystems.

Acknowledgements

First and foremost, I would like to offer my sincere gratitude to my supervisor Prof. Luigi Piroddi, whose precious help, expertise, patience and constant support during these months has been essential to the completion of this thesis. I would also like to thank my co-supervisor Prof. Giancarlo Bernasconi for his insightful comments and support throughout these months.

A very special thank you goes out to all the great people I have met during my two years in Como. This experience would not have been the same without you.

Last but not least, I would like to thank my family and friends who have always been there for me.

Contents

List of Figures

List of Tables

Chapter 1

Introduction

Environmental noise is ubiquitous and pervasive in our society. Long-term exposure to high-intensity acoustic noise presents a potential health hazard in the form of noise-induced hearing loss (NIHL), cardiovascular disease, stress, sleep disturbance, childhood cognitive development and annoyance. Major sources of noise pollution include: industrial and agricultural activities, transportation, household items and social events. Noise regulations aim to mitigate the ill effects of noise pollution via efficient urban planning, architectural design and noise control.

The rotating components in vehicles and industrial machinery emit high-decibel low-frequency periodic noise. Long periods of exposure to low-frequency noise may lead to fatigue and loss of concentration, which may result in reduced comfort and occupational accidents. Noise control is thus necessary. Traditional passive noise-control techniques such as enclosures, barriers and silencers are not effective because the wavelengths associated to low-frequency noise are large with respect to the thickness of the acoustic absorbers typically allowed in these applications. In order to attenuate low-frequency periodic noise, active noise control (ANC) techniques have been developed. ANC works by superposition: the undesired noise is cancelled by injecting an anti-noise signal of equal amplitude and opposite phase using a secondary source, such as a loudspeaker. This is called destructive interference. More specifically, a reference microphone picks up a measurement of the noise and the ANC system processes it to generate a driving

signal for the cancelling loudspeaker. An error microphone is placed where the anti-noise signal is injected to monitor the performance of the system. Low-cost and fast computational devices such as digital signal processors (DSPs) are used to implement a wide variety of digital ANC algorithms based on adaptive filters. These filters are employed as controllers to drive the secondary source and they are often based on variations of the Least Mean Squares (LMS) algorithm, such as the Filtered-x Least Mean Squares (FxLMS) algorithm. FxLMS compensates the phase delays introduced by the measurement and control chain by convolving the reference signal with a finite impulse response (FIR) estimate of the so-called *secondary path*. The performance and stability of FxLMS-based ANC systems depends largely upon the secondary path and its estimate.

Since most of the spectral power in the applications mentioned above is concentrated in the harmonic components of the noise, narrowband ANC techniques have been developed to attenuate those components. Narrowband ANC systems inject synthesised sine waves (the *reference signals*) which are adaptively phase shifted and amplified to control corresponding harmonics in the undesired noise. The parallel-form narrowband ANC system based on Widrow's adaptive notch filter [1] convolves each sinusoidal reference signal with an estimate of the secondary path in order to obtain the filtered-reference signals necessary for the FxLMS algorithm [2]. Moreover, since the environment is often time varying in industrial workplaces or aircraft cabins, narrowband ANC systems include a subsystem that updates the secondary-path estimate during the operations of the system to avoid instability.

The narrowband ANC system based on Widrow's adaptive filter and the FxLMS algorithm offers fast and effective narrowband attenuation, but the reference-filtering operations determine a computational cost that grows linearly with both the order of the FIR secondary-path estimate and the number of controlled harmonics. Therefore, the computational cost associated to the reference-filtering operations may become a performance bottleneck in the implementation of the system. Moreover, the online-modelling subsystem is often quite slow in adapting the secondary-path estimate due to the high order of the estimate, which may render the system unstable if the

estimation errors exceed the stability condition. Finally, since it is impractical to manually set a step size for each adaptive narrowband controller, narrowband ANC systems often rely on the normalised FxLMS algorithm, which further increases their computational cost.

Systems have been proposed in the literature to reduce the computational burden of the parallel-form narrowband ANC system and to offer the same performance in terms of noise cancellation and speed of convergence. In 1989 [3] Ziegler developed a narrowband ANC system that compensates the delay introduced by the secondary path by estimating the integer phase delay it introduces on the controlled harmonics, so that the reference-filtering operations only consist in a time delay. This system is computationally very efficient but the estimation errors limit its convergence speed and noise cancellation. More recently [4] Xiao proposed a system where the reference signals are summed, their sum is convolved with the secondary-path estimate and each filtered reference signal is retrieved by filtering the convolved signal through a bank of bandpass filters. While not computationally as efficient as Ziegler's system, Xiao's system only performs one reference-filtering operation regardless of the number of controlled harmonics and maintains the same convergence-speed and noise-cancellation properties of the original system in many situations. However, it relies on the correct *a priori* choice for a bandwidth-control parameter of the bandpass filters to separate the filtered reference signals, especially if their frequencies are close: if this parameter is too small, the system may be unstable; if it is too large, the system may exhibit slow convergence.

In this thesis, a novel cost-effective approach to the compensation of the delays introduced by the secondary path in narrowband ANC systems is proposed. Instead of using a single global high-order FIR model, we investigate how multiple local lower-order FIR models (called *local secondary paths*) may be employed to obtain the filtered reference signals. A computational analysis establishes that the proposed system reduces the number of required computations with respect to the original system. Simulations show that the proposed system offers comparable convergence speed and noise cancellation with respect to the original system and that it outperforms Ziegler's and Xiao's systems in situations that are critical for those

systems. Furthermore, simulations show that the online modelling of local secondary paths is more reactive to changes in the secondary path than the global online-modelling system thanks to the low order of the local estimates. This increased reactivity makes the system less prone to instability if the environment changes fast. Finally, we provide an empirical step size-correction law that is equivalent to the normalised FxLMS algorithm and less computationally demanding.

The thesis is organised as follows. Chapter 2 contains a review of ANC methods with a focus on narrowband systems and their limits. An overview of the recent research in narrowband ANC is presented. A thorough bibliographic research on one of the most successful ANC applications, namely noise-cancelling headsets, is also provided. In Chapter 3 the proposed system based on the identification of local secondary paths is introduced and discussed, together with the online-modelling subsystem and the step size-correction law. In Chapter 4 the proposed system, Ziegler's system and Xiao's system are analysed and tested against the traditional system. Computational analyses are provided to assess the reduction in computational cost allowed by the evaluated systems. Simulations are carried out to determine how the speed of convergence and noise cancellation of the evaluated systems compares to the traditional system. Chapter 5 reports the conclusions and future research directions.

Chapter 2

State of the art

2.1 A taxonomy of noise-cancelling methods

Acoustic noise can be controlled using passive-cancellation techniques such as enclosures, barriers and silencers. These devices combine different absorbing materials in order to reduce the unwanted interference and they can achieve high attenuation over a broad frequency range at the cost of using thicker materials. For this very reason however, in many practical applications where the controller cannot afford to be bulky (e.g. headsets, helmets, cars or planes), passive techniques fail to remove low frequencies effectively.

As a consequence, active noise control (ANC) techniques were devel-

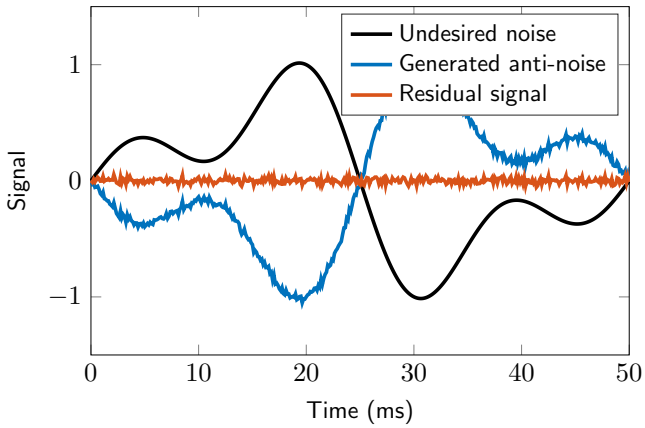

Figure 2.1: Destructive interference.

oped; ANC works by superposition: the undesired noise is cancelled by injecting an anti-noise signal of equal amplitude and opposite phase using an electroacoustic or electromechanical actuator. This phenomenon is called destructive interference (Figure 2.1). The main advantages of active control technologies over passive methods are the reduced cost and the improvements in low-frequency attenuation. Therefore many commercial noise-removal systems combine passive and active techniques.

The first acoustic ANC system was patented in 1936 by Lueg [5]. This analogue system was composed of a microphone and an electronically driven loudspeaker that generated a cancelling sound. Figure 2.2a shows the single-channel duct-acoustic ANC setting: a reference microphone measures the primary noise within the duct, which is then processed by the ANC system to generate the driving signal for the cancelling loudspeaker. Finally, the primary noise and cancelling signal sum up at the error-microphone location. The objective of the ANC controller is to minimise the residual noise contained in the error signal. This setting can be interpreted as a system-identification problem as shown in Figure 2.2b, where an adaptive filter $W(z)$ estimates an unknown time-varying plant $P(z)$, which represents the acoustic response from the reference microphone to the error microphone, so that the error signal may be minimised. It should be noted that this scheme is applicable to a large variety of acoustic problems.

The advent of fast and low-cost computational devices such as digital signal processors (DSPs) has made the digital implementation of active controllers possible. Although digital systems suffer from the delay introduced by the analogue-to-digital and digital-to-analogue converters and the phase delay introduced by the antialiasing low-pass filter, which degrade both the control bandwidth and the attenuation level, they allow the implementation of adaptive algorithms, so that issues related to time-varying and non-stationary noise sources or environments may be tackled effectively.

Most adaptive digital controllers are based on variations of the Least Mean Squares (LMS) algorithm, a stochastic gradient descent method widely used in many fields of engineering because of its effectiveness and relatively low computational cost. Other algorithms commonly used in the field of ANC are based on infinite impulse response (IIR), lattice and transform-

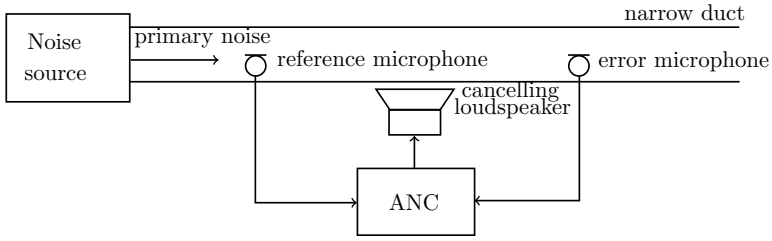

(a) The narrow-duct ANC physical system.

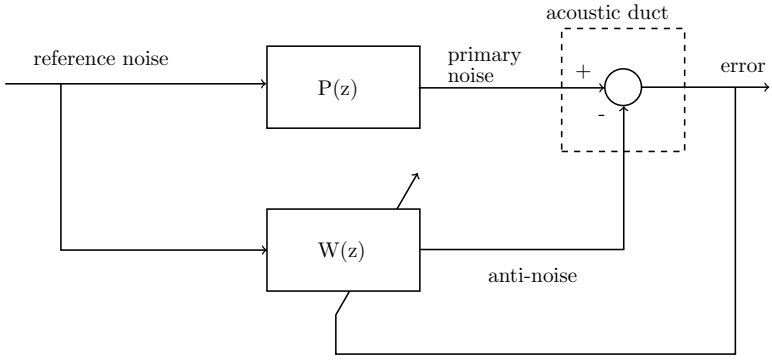

(b) The equivalent block diagram.

Figure 2.2: A physical ANC system and its equivalent block diagram.

domain filters.

In ANC applications a non-negligible phase delay is introduced by the so-called *secondary path*. This transfer function (Figure 4.1a) accounts for the measurement and control chain at the summing junction, i.e. the digital-to-analogue converter, the reconstruction filter, the power amplifier, the loudspeaker dynamics, the acoustic path from the loudspeaker to the microphone, the error microphone, the preamplifier, the anti-aliasing filter and finally the analogue-to-digital converter (as described in [6]) and it can be compactly modelled by an infinite impulse response (IIR) filter

$$S(z) = \frac{\sum_{i=0}^{P} b_i z^{-i}}{\sum_{j=0}^{Q} a_j z^{-j}}. \tag{2.1}$$

For this reason, variations of the LMS algorithm have been proposed in the ANC literature whose performance depends largely upon the estimation of the secondary path. For example, a zero in the secondary path causes an unobservable and thus uncontrollable frequency component.

Adaptive digital noise cancellers may be based either on feedforward

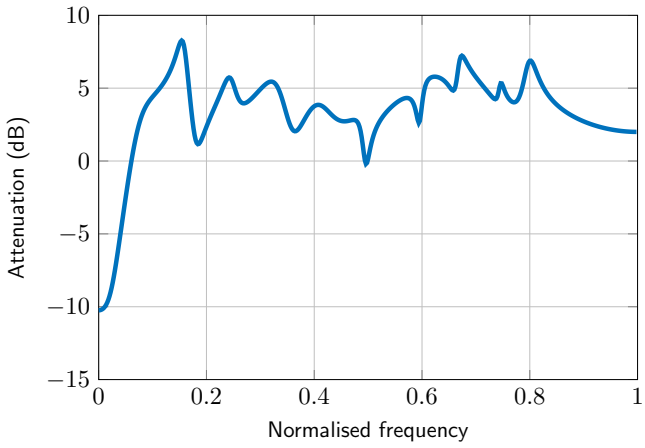

(a) Magnitude response.

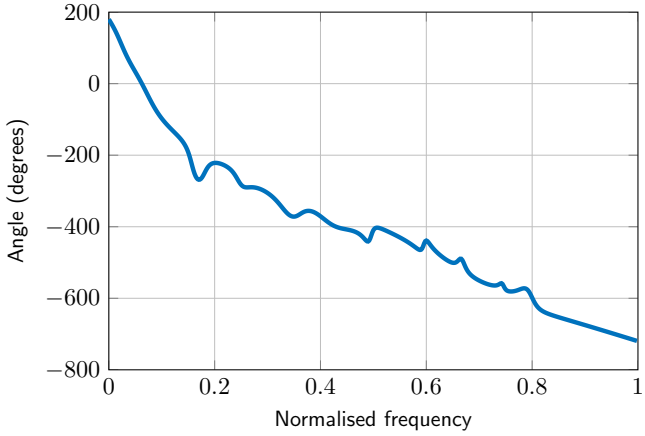

(b) Phase response.

Figure 2.3: A typical secondary path.

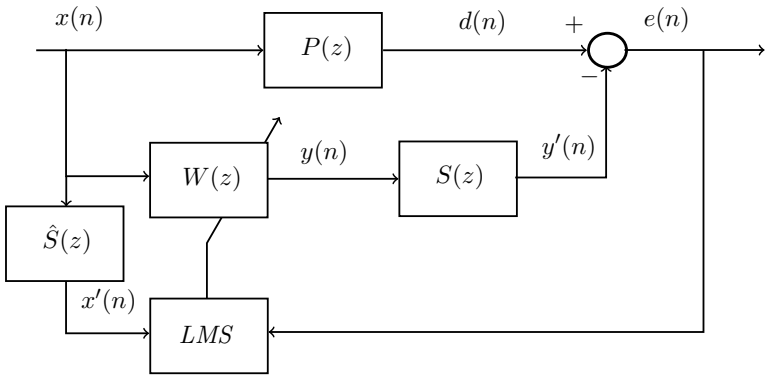

Figure 2.4: Broadband feedforward ANC.

control or on feedback control.

In digital feedforward control systems (Figure 2.4) an external sensor (called *reference microphone*) picks up a measurement of the external noise $x(n)$, which is subsequently filtered by the LMS-based controller $W(z)$ and fed to the loudspeaker. An internal sensor (called *error microphone*) is used to tune the digital filter in order to minimise the error signal $e(n)$ at this location. The adaptive controller $W(z)$ is used to simultaneously estimate the unknown time-varying plant $P(z)$ and invert the secondary path $S(z)$. To achieve this, the most commonly used variation of the LMS algorithm is the so-called filtered-reference LMS (FxLMS) algorithm, which is based on the following update equation:

$$\mathbf{w}(n+1) = \mathbf{w}(n) + \mu \mathbf{x}'(n) e(n), \tag{2.2}$$

where $\mathbf{w}(n) = [w_0(n)\ w_1(n)\ ...\ w_{L-1}(n))]^T$ are the coefficients of the L-order adaptive FIR filter $W(z)$, $\mathbf{x}(n) = [x(n)\ x(n-1)\ ...\ x(n-L+1))]^T$ is the signal vector, $\mathbf{x}'(n) = (\hat{s} * \mathbf{x})(n)$ is the filtered signal vector and $\mu > 0$ is a step size. Refer to [7] for a complete description and analysis of the algorithm.

The main constraint on feedforward ANC systems is that the electrical delay between the two microphones must not exceed the acoustic delay lest the cancellation signal arrive too late to act on the unwanted noise. If that is the case, then only cancellation of periodic (i.e. predictable) noise can be achieved by feedforward systems.

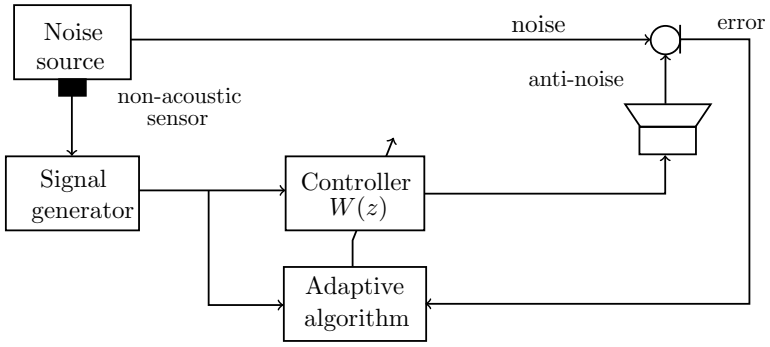

Figure 2.5: General narrowband ANC scheme using a non-acoustic sensor to estimate the frequency of the sinusoidal interferences.

A problem this system may suffer from is acoustic feedback, which happens when the generated anti-noise signal radiates upstream to the primary microphone. This may lead to instability or performance degradation and variants of the FxLMS algorithm have been proposed to solve this problem. For example, the so-called filtered-u LMS (FuLMS) algorithm was proposed by Eriksson in [8].

This feedforward configuration (sometimes called *broadband ANC*) is fastest when controlling flat-spectrum noise signals such as white noise, but works in principle on any kind of noise. When the noise to be removed is periodic however, a single-microphone feedforward configuration may be used.

Narrowband ANC systems (Figure 2.5) control harmonic sources by adaptively filtering an internally generated reference signal. The signal generator is triggered by a non-acoustic sensor (such as a tachometer) and the produced reference signal can either be a train of impulses (*waveform synthesis*) or a sine wave (*adaptive notch filter*).

A digital feedback control system (Figure 2.6) works like a broadband feedforward system that synthesises its reference signal based on the adaptive filter output and the error signal, thus avoiding acoustic feedback entirely. The main advantages of this configuration are its compactness, low cost and effectiveness at controlling harmonic noise.

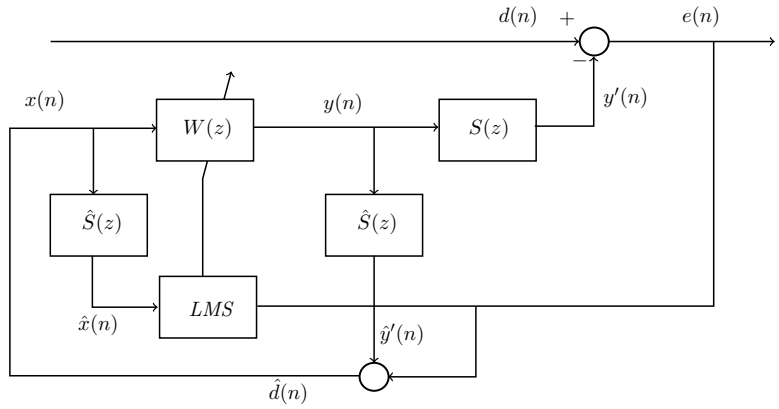

Figure 2.6: Broadband feedback ANC.

2.1.1 On stability and convergence speed

The theoretical analysis of the FxLMS algorithm in the broadband feedforward-control case (Figure 2.4) highlights that both the stability and the performance of the FxLMS algorithm depend on the secondary path [6]:

Stability A frequency-domain analysis of the time-domain behaviour of the FxLMS algorithm shows that stability is ensured as long as the phase error between the estimated secondary path and the actual secondary path stays below 90° at all frequencies.

Performance The convergence speed of the FxLMS algorithm depends instead on the eigenvalue spread of the autocorrelation matrix $\mathbf{R}$, defined as $\mathbf{R} = E[\mathbf{x}(n)\mathbf{x}(n)^T]$; the larger the eigenvalue spread, the longer the convergence time. As a consequence, flat-spectrum signals such as white noise show fastest convergence. Moreover, despite the algorithm robustness to secondary-path estimation errors both in phase and magnitude, these errors do slow down the adaptation process.

For these reasons, the secondary path is estimated offline prior to the operations of the ANC system. However, if the environment changes, the secondary-path phase response might change by more than 90°, making the FxLMS algorithm unstable. Hence, the secondary-path estimate must be updated when the ANC system is operating to ensure both stability and performance.

Several techniques have been proposed to tackle the time variance of the secondary path: some are based on the injection of an excitation signal in the system to update the secondary-path estimate online, others exploit application-specific characteristics of the problem to avoid instability. See [7] for an in-depth overview of secondary-path online modelling techniques.

2.2 A focus on narrowband ANC

In many applications the undesired noise has a periodic nature if the noise source is related to rotating machinery, such as engines, compressors, motors, fans, propellers, etc. Air-acoustic ANC systems can therefore employ a non-acoustic sensor (e.g. an accelerometer, a tachometer or an optical sensor) to estimate the fundamental frequency of the noise and generate a reference signal that is unaffected by the acoustic actuator radiating upstream to the sensor.

As shown in Figure 2.5, the system filters the synthesised reference signal $x(n)$ through $W(z)$ to produce a cancelling signal $y(n)$ and adapts the digital controller $W(z)$ with an error microphone placed in the noise field. This technique has the following advantages [6]:

- The acoustic feedback problem of feedforward broadband ANC systems is avoided.
- The periodicity of the noise removes allows longer controller delays.
- Using synthesised reference signals allows the independent control of each periodic component.
- Lower-order controllers may be used since the acoustic path transfer functions only need to be modelled in a neighbourhood of the harmonic tones, which results in computational efficiency.
- Typical problems associated with acoustic sensors, such as nonlinearities and aging, are avoided (e.g. the high temperatures found in engine exhausts can make it difficult to retrieve an acoustic measurement of the noise).

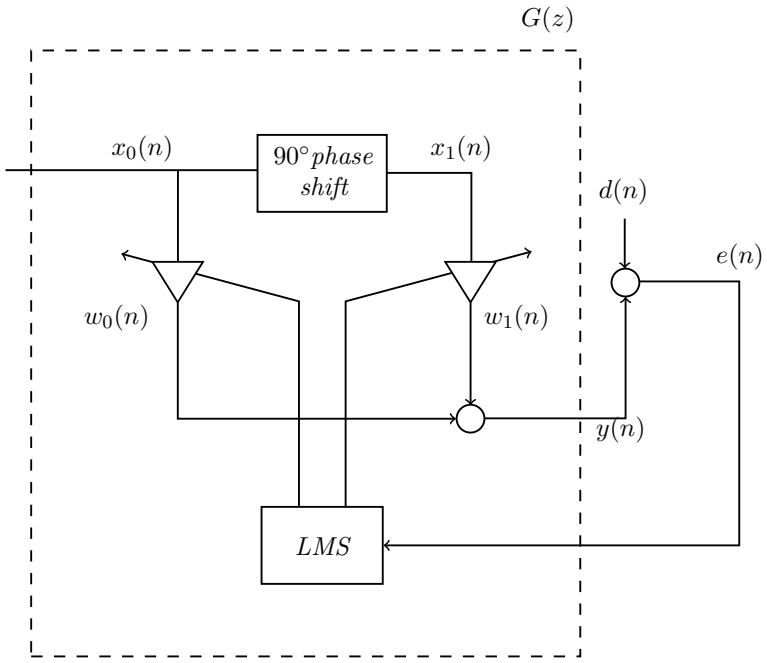

Figure 2.7: Widrow's sinusoidal canceller or adaptive notch filter.

Two classic narrowband ANC techniques are the waveform synthesis and the adaptive notch filter. The first method uses a train of impulses whose period is equal to the inverse of the fundamental frequency of the harmonic noise as its reference signal. The second method uses synthesised sinusoidal signals that have the same frequencies as the harmonic tones to be cancelled. Our focus will be on the latter, since waveform synthesis only works under very constrained conditions [7].

The single-frequency adaptive notch filter was first proposed in 1975 by Widrow [1] as a way to cancel sinusoidal interferences from a given signal. Applications of this technique were later formulated in the context of narrowband ANC [3] [2].

2.2.1 Narrowband adaptive sinusoidal canceller

The basic idea behind the single-frequency adaptive notch filter as proposed by Widrow is that by injecting a sine wave and adaptively tuning its phase and amplitude the filter can cancel a sinusoidal interference at a specific frequency (Figure 2.7). In fact, any signal $u(n)$ corrupted by a sinusoidal

interference at frequency f_0 can be written as

$$d(n) = a_n \cos(2\pi f_0 n) + b_n \sin(2\pi f_0 n) + u(n). \tag{2.3}$$

The controller injects a linear combination of the reference signal $x_0(n) = A\cos(2\pi f_0 n)$ and its phase-shifted version $x_1(n) = A\sin(2\pi f_0 n)$ at the control point

$$y(n) = w_0(n)x_0(n) + w_1(n)x_1(n), \tag{2.4}$$

and uses the error signal $e(n) = d(n) - y(n)$ to tune the two adaptive coefficients $w_0(n)$ and $w_1(n)$ so that they converge to the two Fourier coefficients of the interference scaled by the reference-signal amplitude (respectively $\frac{a_n}{A}$ and $\frac{b_n}{A}$). The adaptation is based on the LMS update law:

$$w_i(n+1) = w_i(n) + \mu x_i(n)e(n) \qquad i = 0,\ 1. \tag{2.5}$$

After convergence, the residual error is

$$e(n) \approx u(n) \tag{2.6}$$

and the controller will try to track any phase or magnitude change that may occur in the sinusoidal interference.

It can be shown that after convergence the transfer function from $e(n)$ to $y(n)$ is equivalent to

$$G(z) \approx \mu A^2 \frac{z\cos(2\pi f_0) - 1}{z^2 - 2z\cos(2\pi f_0) + 1}. \tag{2.7}$$

This transfer function has two complex-conjugate poles on the unit circle at $z = e^{\pm j2\pi f_0}$ and a real zero at $z = \frac{1}{\cos(2\pi f_0)}$.

The steady-state transfer function $H(z)$ from the corrupted primary input $d(n)$ to the error signal $e(n)$ is

$$H(z) = \frac{E(z)}{D(z)} = \frac{1}{1 + G(z)} = \frac{z^2 - 2z\cos(2\pi f_0) + 1}{z^2 - (2 - \mu A^2)z\cos(2\pi f_0) + 1 - \mu A^2}. \tag{2.8}$$

The zeros of $H(z)$ are the poles of $G(z)$ and its poles are located roughly at the same angle of the zeros but inside the unit circle (provided that μ is small enough). It can be proven that the stability condition is

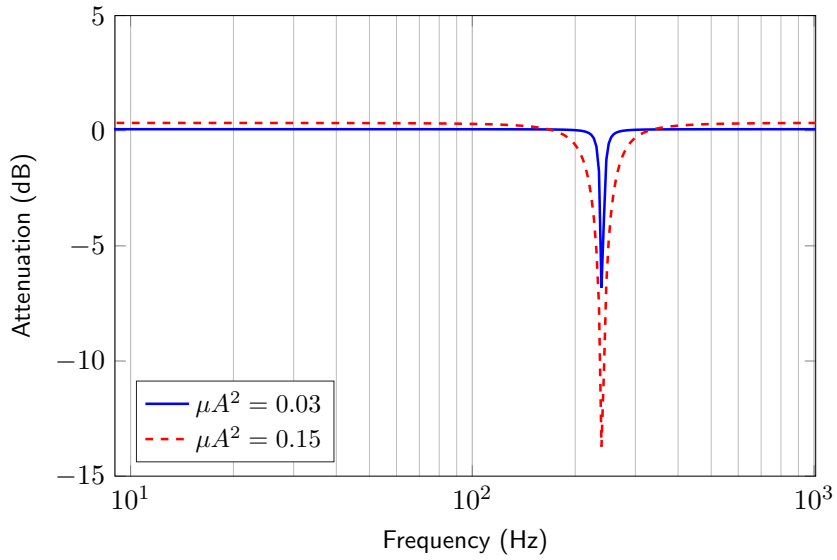

Figure 2.8: The bandwidth of the adaptive notch filter depends on the μA^2 gain.

$$0 < \mu < \frac{2}{A^2}. \tag{2.9}$$

Since the zeros lie on the unit circle, the filter achieves an infinite null at the frequency f_0. The sharpness of the notch depends on the μA^2 factor, which determines the closeness of the poles to the unit circle. Figure 2.8 shows a typical frequency response of the adaptive sinusoidal canceller. Using a larger step size has the effect of providing wider notches and faster tracking of jittering frequencies.

A convergence analysis of the LMS algorithm shows that the adaptive notch filter exhibits very fast convergence since the eigenvalue spread of the autocorrelation matrix equals one. Variations of this algorithm employing non-orthogonal reference signals, such as $x_0(n) = A\cos(2\pi f_0 n)$ and $x_1(n) = x_0(n-1)$, will exhibit a slower convergence but will converge nonetheless.

This controller cannot be applied to ANC problems as is because it does not account for the phase delay and amplitude change introduced by the secondary path. We will present in the following sections two modifications to Widrow's adaptive notch filter, where the sinusoidal reference signals are convolved with an estimate of the secondary path so that the FxLMS algorithm may be used. The first method estimates $S(z)$ with an FIR filter

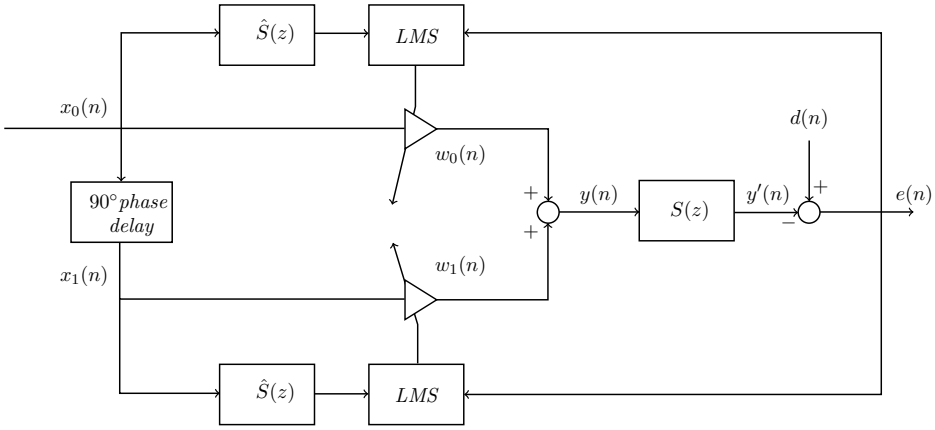

Figure 2.9: Adaptive notch filter with the FxLMS algorithm.

$\hat{S}(z)$, while the second method estimates the phase delay Δ introduced by $S(z)$ exactly at the controlled frequency and delays the reference signal accordingly. The first approach yields good noise-attenuation results but is computationally demanding because it requires a high-order FIR estimate to operate correctly and ensure stability; viceversa, the second approach is computationally very efficient but does not perform as well because the estimated phase delay is never exact in practice.

2.2.2 Single-frequency ANC using the filtered-reference LMS algorithm (traditional system)

A popular approach for the compensation of the secondary path is to employ a global secondary-path estimate $\hat{S}(z)$, as in the FxLMS algorithm [2] (Figure 2.9). The adaptive weights are updated as

$$w_i(n+1) = w_i(n) + \mu x_i'(n) e(n) \qquad i = 0,\ 1 \tag{2.10}$$

where $x_0'(n)$ and $x_1'(n)$ are the filtered versions of the two reference signals through the secondary-path model $\hat{S}(z)$.

If the primary input can be written as

$$d(n) = A_d \cos(2\pi f_0 n + \Phi_d) \tag{2.11}$$

and the injected control signal as

$$y(n) = (x_0 * w * s)(n) = AA_w A_s \cos(2\pi f_0 n + \Phi_w + \Phi_s) \tag{2.12}$$

then the error signal is

$$e(n) = A_d \cos(2\pi f_0 n + \Phi_d) - AA_w A_s \cos(2\pi f_0 n + \Phi_w + \Phi_s), \tag{2.13}$$

where $A_w = \left|W(e^{j2\pi f_0})\right|$, $\Phi_w = \angle W(e^{j2\pi f_0})$ and similarly A_s and Φ_s denote respectively the amplitude and phase of the secondary path at frequency f_0.

Therefore, the optimal controller, in order to minimise the error signal, will adapt the filter weights so that

$$A_w = \frac{A_d}{AA_s} \tag{2.14}$$

and

$$\Phi_w = \Phi_d - \Phi_s, \tag{2.15}$$

i.e. it will tune the phase and magnitude of the injected signal to both compensate for the amplitude and phase shift introduced by the secondary path (inversion of $S(z)$) and identify the amplitude and phase of the undesired periodic interference (modelling of $P(z)$).

It can be proven that in the limit of slow adaptation the transfer function from $d(n)$ to $e(n)$ becomes

$$H(z) = \frac{z^2 - 2z\cos(2\pi f_0) + 1}{z^2 - [2\cos(2\pi f_0) - \beta\cos(2\pi f_0 - \Phi_\Delta)]z + 1 - \beta\cos\Phi_\Delta} \tag{2.16}$$

where $\Phi_\Delta = \Phi_S - \Phi_{\hat{S}}$ is the phase difference between $S(z)$ and $\hat{S}(z)$ at f_0 and $\beta = \mu A^2 A_s$. $H(z)$ notches at f_0 and is stable if and only if

$$-90^\circ < \Phi_\Delta < 90^\circ, \tag{2.17}$$

i.e. when the secondary-path phase estimation error is limited between $\pm\frac{\pi}{2}$. This stability condition is the same as the one found for the broadband feedforward configuration.

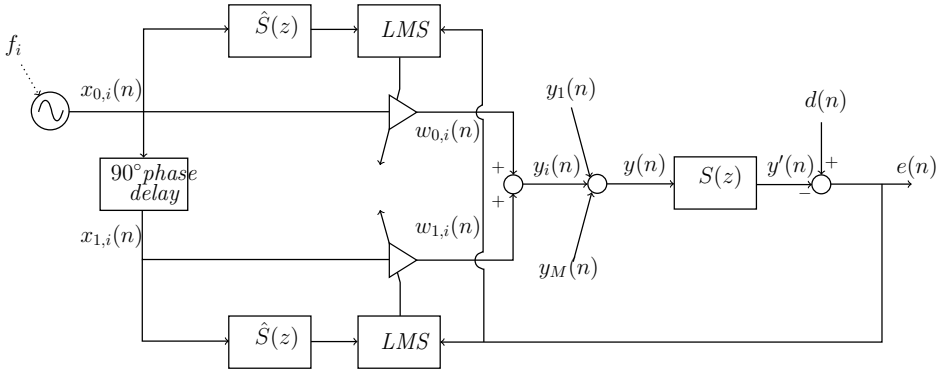

Figure 2.10: Parallel-form narrowband ANC.

2.2.3 Multiple-frequency ANC using the filtered-reference LMS algorithm

When the sinusoidal interference is multi-harmonic, i.e.

$$d(n) = \sum_{i=0}^{M-1} (a_i \cos(2\pi f_i n) + b_i \sin(2\pi f_i n)) + u(n), \tag{2.18}$$

different approaches may be tried [6]:

- A signal containing multiple frequencies (such as a sum of sinusoids, a square wave, a triangular wave, etc) may be employed as the excitation signal. This method has several drawbacks, such as the need to use a higher-order adaptive controller and one single step size which makes it virtually impossible to control each interference independently.

- Single-frequency narrowband ANC systems may be connected in cascade, but this structure suffers from the increase in computational cost and convergence speed each time a further stage is added.

- Finally, single-frequency narrowband cells may be connected in parallel, which is the most commonly studied configuration in the narrowband ANC literature for its simplicity and effectiveness at controlling multiple harmonics.

The block diagram for the parallel configuration is shown in Figure 2.10.

Each single-frequency ANC controller is connected in parallel and their outputs

$$y_i(n) = w_{0,i}(n)x_{0,i}(n) + w_{1,i}(n)x_{1,i}(n) \qquad i = 0,\ \ldots,\ M-1 \tag{2.19}$$

are summed into

$$y(n) = \sum_{i=0}^{M-1} y_i(n), \tag{2.20}$$

which is subsequently fed to the loudspeaker at the control point.

The adaptive coefficients are updated using a single error signal $e(n)$ according to the FxLMS algorithm

$$w_{0,i}(n+1) = w_{0,i}(n) + \mu_i x'_{0,i}(n)e(n) \qquad i = 0,\ \ldots,\ M-1, \tag{2.21a}$$

$$w_{1,i}(n+1) = w_{1,i}(n) + \mu_i x'_{1,i}(n)e(n) \qquad i = 0,\ \ldots,\ M-1 \tag{2.21b}$$

where $x'_{0,i}(n)$ and $x'_{1,i}(n)$ are the filtered reference signals and μ_i are the step sizes of each narrowband ANC block.

Since the secondary path attenuates some frequencies and amplifies some others according to its resonances, when the reference signals are convolved with the secondary-path estimate they are scaled by the magnitude value of the transfer function at the controlled frequency. This effectively scales the step size. In fact, the FxLMS update rule for the first coefficient becomes

$$\begin{aligned} w_{0,i}(n+1) &= w_{0,i}(n) + \mu_i x'_{0,i}(n)e(n) = \\ &= w_{0,i}(n) + \mu_i A_{\hat{S}} A\cos(2\pi f_i n + \Phi_{\hat{S}})e(n) \\ &\qquad i = 0,\ \ldots,\ M-1 \end{aligned} \tag{2.22}$$

where $A_{\hat{S}} = \left|\hat{S}(e^{j2\pi f_i})\right|$ and $\Phi_{\hat{S}} = \angle\hat{S}(e^{j2\pi f_i})$ and similarly for the second coefficient. Let us remind that by reducing the step size convergence slows down and conversely by increasing the step size the convergence time decreases.

Using a parallel configuration when controlling multiple harmonics offers a great deal of flexibility in this respect, thanks to the fact that each narrowband block can use a different step size μ_i to compensate for this scaling. Multiple-frequency narrowband ANC systems that use a single reference signal containing all the harmonics to be controlled (e.g. a rectangular wave) and a single controller, instead, are forced to use a single step size for all narrowband components. This entails balancing two conflicting goals. On the one hand, a large step size is needed to compensate for the performance drop due to the attenuation of some frequencies. On the other hand, a large step size can be further magnified if the secondary path has a resonance around one of the controlled frequencies, which may destabilise the entire system. Parallel systems do not have to deal with this tradeoff because each step size μ_i may be chosen independently from the others.

Since in practice it is not trivial to choose a step size for each controlled harmonic *a priori*, most systems either use the same step size for all controlled frequencies or they implement the normalised version of the FxLMS algorithm:

$$w_{0,i}(n+1) = w_{0,i}(n) + \frac{\mu_i x'_{0,i}(n) e(n)}{x'_{0,i}(n)^2 + \epsilon} \qquad i = 0,\ \ldots,\ M-1, \tag{2.23a}$$

$$w_{1,i}(n+1) = w_{1,i}(n) + \frac{\mu_i x'_{1,i}(n) e(n)}{x'_{1,i}(n)^2 + \epsilon} \qquad i = 0,\ \ldots,\ M-1, \tag{2.23b}$$

where ϵ is a small regularisation term and μ_i in this case is the normalised step size. This removes the need to manually tune every step size, but it comes at the cost of additional multiplications that increase linearly with the number of controlled harmonics.

Another problem of the parallel-form ANC system is the computational cost of convolving each reference signal with the secondary-path estimate $\hat{S}(z)$, whose order L' in many practical situations must be quite large to provide a decent approximation of the secondary path: increasing the number of controlled harmonics M results in a linear increase in the computational load. In particular, the overall system performs ML' multiplications per iteration to obtain the filtered reference signal of each narrowband ANC unit.

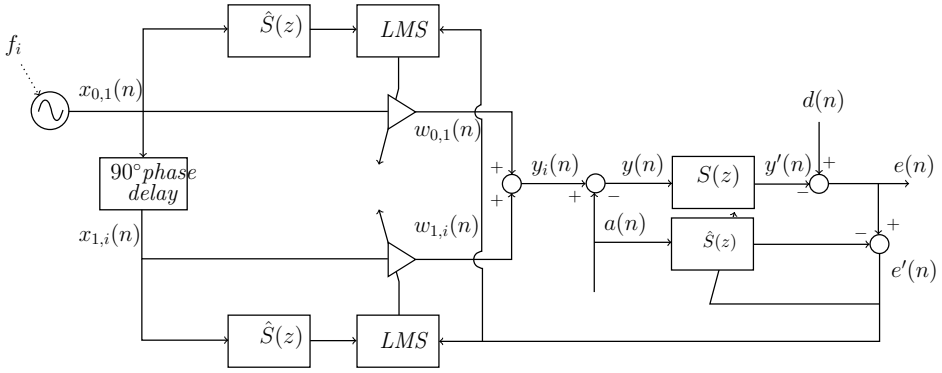

Figure 2.11: Parallel-form narrowband ANC with online modelling. This system can also perform offline modelling when the ANC units are switched off ($y_i(n) \equiv 0 \ \forall i, \ n$).

2.2.4 Multiple-frequency ANC using the filtered-reference LMS algorithm with online modelling of the secondary path

In general, the secondary path $S(z)$ does not remain constant in time because the environment in many ANC applications is time-varying. This means that the estimate $\hat{S}(z)$, which is learnt prior to the operations of the system, may diverge from $S(z)$ to the point of instability. To avoid this from happening, an online-modelling subsystem may be added to the ANC scheme. Many online-modelling schemes have been proposed in the literature, such as the one shown in Figure 2.11.

A broadband exciting signal (such as white Gaussian noise) $a(n)$ of variance σ_a^2 is injected into the system at the control point:

$$y(n) = \sum_{i=0}^{M-1} y_i(n) - a(n). \tag{2.24}$$

The secondary-path model is updated using the signal

$$e'(n) = e(n) - a'(n) \tag{2.25}$$

with the FxLMS algorithm:

$$\hat{\mathbf{s}}(n+1) = \hat{\mathbf{s}}(n) + \mu_s \mathbf{a}(n) e'(n) \tag{2.26}$$

where

- $\hat{\mathbf{s}}(n) = [\hat{s}_0(n)\ \hat{s}_1(n)\ \ldots\ \hat{s}_{L'-1}(n)]^T$ is the impulse response of the secondary-path estimate $\hat{S}(z)$,
- $\mathbf{a}(n) = [a(n)\ a(n-1)\ \ldots\ a(n-L'+1)]^T$ is the excitation-signal vector and
- μ_s is the step size.

If we turn off the ANC units ($\mu_i = w_{j,i}(n) = 0\ \forall i,\ j,\ n$), the z transform of $e'(n)$ becomes

$$E'(z) = D(z) + \left(S(z) - \hat{S}(z)\right) A(z), \tag{2.27}$$

whose minimum (when minimising with respect to $\hat{S}(z)$) is reached for $\hat{S}(z) = S(z)$.

Similarly, $e'(n)$ should be used when adapting the ANC filters instead of $e(n)$ because, once the secondary-path model has converged to its optimal solution and the ANC units have been switched on, we have that

$$E'(z) \approx D(z) - \sum_{i=0}^{M-1} S(z)Y_i(z), \tag{2.28}$$

which is equivalent to the expression for $E(z)$ in the system without online modelling, whereas

$$E(z) = D(z) - \sum_{i=0}^{M-1} S(z)Y_i(z) + S(z)A(z) \tag{2.29}$$

contains the online-modelling excitation signal which would disturb and slow down (or possibly bias) the convergence of the ANC units. The formula also highlights that the variance of the excitation signal $a(n)$ must be kept small because, despite not disturbing the convergence of the ANC filters once $\hat{S}(z)$ has converged, $a(n)$ is heard at the control point and thus influences the achievable noise-attenuation level.

Online modelling algorithms can adapt the secondary-path estimate when $S(z)$ is slowly varying, but they may become unstable when the changes are abrupt and large. For this reason, application-specific approaches have been proposed in the literature. However, even when the changes are not abrupt,

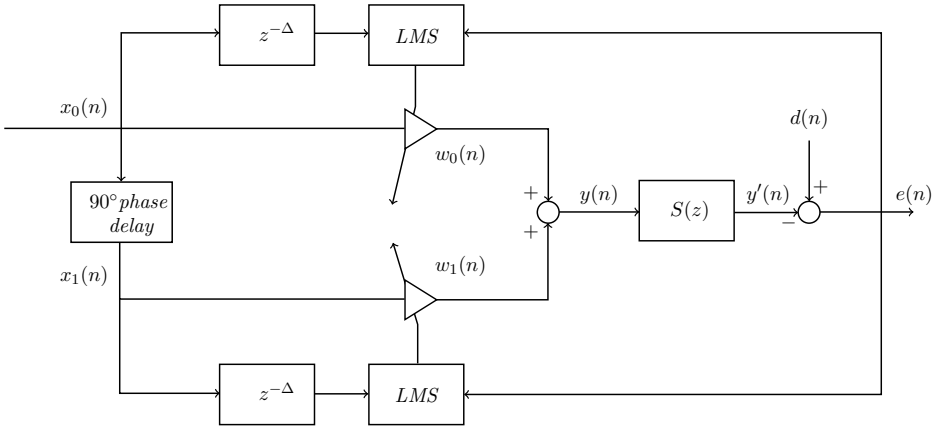

Figure 2.12: Ziegler's adaptive filter with secondary path-delay compensation.

online-modelling algorithms may fail to update $\hat{S}(z)$ fast enough before $S(z)$ changes further, which may allow the phase error between $S(z)$ and $\hat{S}(z)$ to grow beyond 90°. This is due to the fact that the step size for online modelling, and therefore the convergence speed of the online-modelling subsystem, is constrained by the large order L' of $\hat{S}(z)$:

$$\mu_s < \frac{0.1}{L'\sigma_a}. \tag{2.30}$$

2.2.5 Single-frequency ANC using delay compensation (Ziegler's system)

Another application of Widrow's adaptive notch filter to narrowband ANC was developed by Ziegler in 1989 [3] (Figure 2.12). The proposed system compensates for the secondary-path transfer function by estimating the phase delay it introduces at the controlled frequency f_0.

The LMS algorithm updates the filter weights to minimise the residual error $e(n)$:

$$w_i(n+1) = w_i(n) + \mu x_i(n-\Delta)e(n) \qquad i = 0,\ 1. \tag{2.31}$$

This update law can be interpreted as a particular case of the FxLMS algorithm where the secondary-path estimate is $\hat{S}(z) = z^{-\Delta}$.

Since in general the phase delay depends on the frequency to be controlled, the phase-dependent phase lag $\Delta(f)$ can be computed by taking the

discrete Fourier transform of the secondary-path impulse response, computing the phase delay

$$\tau(f) = -\frac{\angle \hat{S}(f)}{2\pi f}, \tag{2.32}$$

where $\angle \hat{S}(f)$ represents the phase response of the secondary path evaluated at frequency f, and finally by approximating the phase lag as

$$\Delta = nint\left[\frac{\tau(f_0)}{T_s}\right] \tag{2.33}$$

where T_s is the sampling period and $nint$ is the nearest-integer function.

Since the phase lag Δ must be integer, the delay compensation introduced by the $z^{-\Delta}$ block will not in general be the same phase delay introduced by the actual secondary path $S(z)$. This is especially aggravated as the sampling frequency gets smaller since the choice for phase lags becomes more coarse-grained and this causes larger estimation errors. For this reason, Ziegler's controller, while computationally very efficient with respect to the approach based on FxLMS since it requires no multiplications to obtain its equivalent filtered reference signals $x_0(n-\Delta)$ and $x_1(n-\Delta)$, will perform worse because a phase error in the estimation of the secondary path is always present in practice.

2.3 Limits of narrowband ANC systems: frequency control and frequency estimation

Narrowband ANC systems based on Widrow's adaptive notch filter outperform broadband techniques when the undesired noise is multi-harmonic, but this advantage comes at the significant cost of frequency estimation; in fact, the signal generator must know the frequency (frequencies) of the periodic interference (interferences) in order to synthesise the correct reference signal and an error in the frequency estimation degrades the achievable noise attenuation, because Widrow's filter exhibits a perfect null only at the estimated frequency.

Since engine-produced frequencies at steady state tend to fluctuate to some extent and slight errors in the frequency estimation are always present

in practice, due, if nothing else, to the finite-precision arithmetics of the processor, the theoretical analysis of the performance and stability of the adaptive notch filter in the case of frequency mismatch (FM from now on) is important.

The 3-dB bandwidth of the notch filter can be estimated as [9]

$$B \approx \frac{\mu A^2}{2\pi T_s}, \tag{2.34}$$

where μ is the step size, A is the amplitude of the reference signal and T_s is the sampling period. Thus, a first rough but effective method for improving the attenuation when FM occurs is to choose a larger step size within the limits of stability.

Equation 2.34 also highlights another important property of the adaptive notch filter: the out-of-band attenuation is directly proportional to the sampling frequency. In fact, while in the ideal case the adaptive weights converge to a constant solution, in the case of FM they converge to an oscillating solution in order to make up for the frequency-estimation error: a larger sampling frequency gives the system more leeway for this adjustment.

The actions that can be taken to improve FM attenuation on the controller side are therefore limited by the very nature of the adaptive notch filter. For this reason, it is important to design a robust and precise frequency estimator. Some solutions in this area include:

Hardware-based approach Use an external hardware device such as an tachometer or phase-locked loops (PLL's) to provide a reliable estimation of the fundamental frequency.

Adaptive algorithms Adaptive frequency trackers have been developed in the literature, such as Regalia's lattice-based IIR adaptive notch filter [10]. These algorithms often find difficulties in tracking multiple frequencies however.

Pitch detection algorithms Non-adaptive frequency trackers may also be employed, even though these algorithms must resolve a tradeoff between computational cost and accuracy: for example, the zero-crossing

method is computationally efficient but not reliable in practical applications, while the mel-frequency cepstrum method is accurate but it requires more computations.

2.4 Limits of narrowband ANC systems: time-varying controlled frequencies

So far we have assumed that the frequencies of the reference signals remain constant in time. In practical situations however, periodic interferences tend to vary not only in phase and amplitude but also in frequency. While narrowband ANC systems based on Widrow's adaptive filter can adapt to phase and amplitude changes, they are less effective against frequency mismatch, which inevitably degrades the achievable noise attenuation (see Equation 2.34).

Figure 2.13 shows what happens when the controlled frequency grows smoothly and the reference-signal frequency follows it. In both simulations, the sampling frequency is $F_s = 8000Hz$, the step size is set to $\mu_0 = 0.0028$ and we assumed that the frequency estimator yields the correct value for the controlled frequency at each iteration. Even under this unrealistic hypothesis, the simulations show that when the frequency variation is too steep (as in Figure 2.13b), the system struggles to attenuate the noise when the change is taking place. This suggests that narrowband ANC systems remove noise effectively only when the controlled frequency varies slowly or when it remains constant for long periods of time (e.g. industrial machinery working at steady-state) and, consequently, this suggests that performing frequency estimation at every iteration may be an unnecessary computational cost.

2.5 Recent research in narrowband ANC

Multi-harmonic control and frequency estimation can be seen as two complementary tasks in the field of narrowband ANC. In the following two sections, we will discuss these two problems in the context of the recent literature.

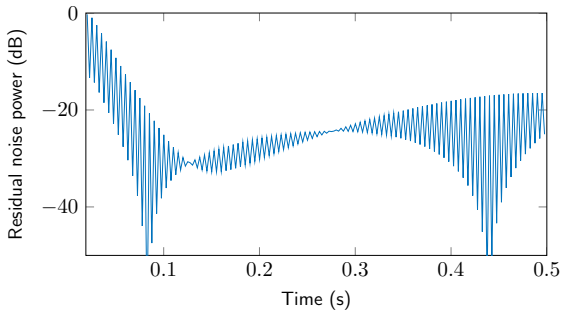

(a) The controlled frequency grows from $f_0 = 300Hz$ to $f_0 = 301Hz$ in $500ms$.

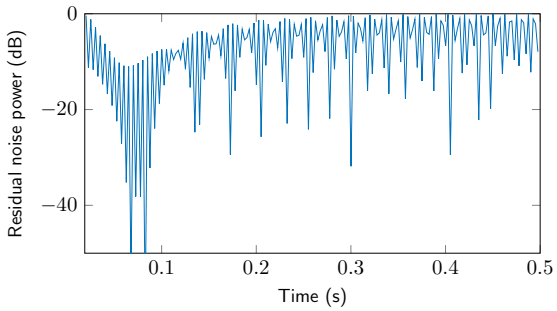

(b) The controlled frequency grows from $f_0 = 300Hz$ to $f_0 = 320Hz$ in $500ms$.

Figure 2.13: Testing the traditional ANC system when the controlled frequency varies smoothly from one value to another in $500ms$.

2.5.1 Modifications of the parallel narrowband ANC controller

2.5.1.1 Xiao's system

As already mentioned in the previous sections, when more than one harmonic noise component must be controlled, each reference signal must be convolved with the secondary-path FIR estimate $\hat{S}(z)$, whose order L' in many practical situations can be quite large to provide a decent approximation of the secondary path (at least one hundred). As a consequence, increasing the number M of controlled harmonics results in a linear increase in the computational load.

In 2008 [4] Xiao proposed a variation of the parallel narrowband ANC system that avoids this computational burden by summing every reference signal, convolving the resulting signal with the secondary-path estimate and

then retrieving each filtered reference signal with a bank of IIR bandpass filters

$$H_{bp,i} = \frac{(\rho - 1)c_i z^{-1} + (\rho^2 - 1)z^{-2}}{1 + \rho c_i z^{-1} + \rho^2 z^{-2}} \qquad i = 0,\ 1,\ \ldots\ M-1, \tag{2.35}$$

where $c_i = -2\cos(2\pi f_i)$ and ρ is a pole-attraction factor. Thus the new system requires fewer multiplications since it only performs one $\hat{S}(z)$ convolution instead of M convolutions per iteration.

However, when two controlled frequencies are close, the bandpass filters struggle to separate their frequency peaks. To do so, they must use a larger ρ, which increases the time constant associated to the bandpass filters. This slows down the convergence as shown in Figures 2.14 and 2.15. Xiao's system takes a longer time to reduce the noise by $20dB$ with respect to the traditional system and its behaviour is very sensitive to the choice of the pole-attraction factor ρ.

2.5.1.2 Chang and Kuo's system

In order to cancel several narrowband components, the parallel-form narrowband ANC system uses a single error signal containing all harmonics to update all adaptive filters. This degrades the convergence speed and thus noise reduction, since the other harmonic components act as a disturbance for every controller.

In 2013 [11] Chang and Kuo developed a parallel narrowband ANC system that uses individual error signals to update the corresponding adaptive filters and thus improves the system's speed of convergence. The system uses a bank of second-order IIR bandpass filters to split the error signal into corresponding channels. The filters are designed to have unity gain and zero phase at the centre of the pass band to avoid introducing an additional delay in the secondary path.

As pointed out in a 2014 correspondence paper however [12] the employed bandpass filters exhibit a peak in the group delay which increases as the bandwidth is decreased. Simulations showed that this overlooked issue appears to limit the convergence speed such that the fastest convergence speed is achieved by the conventional narrowband controller without

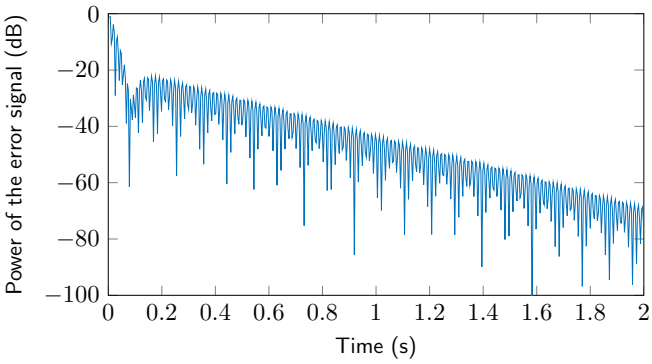

(a) Traditional system based on FxLMS.

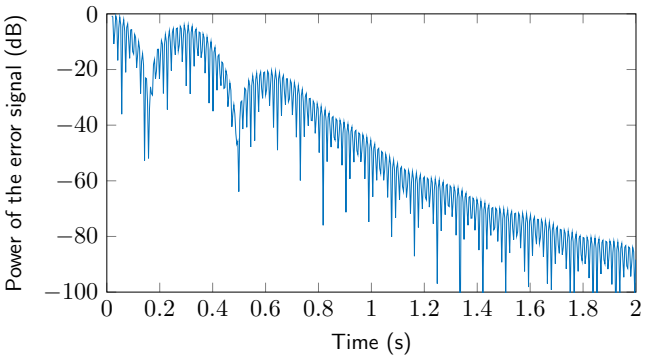

(b) Xiao's system when $\rho = 0.9999$.

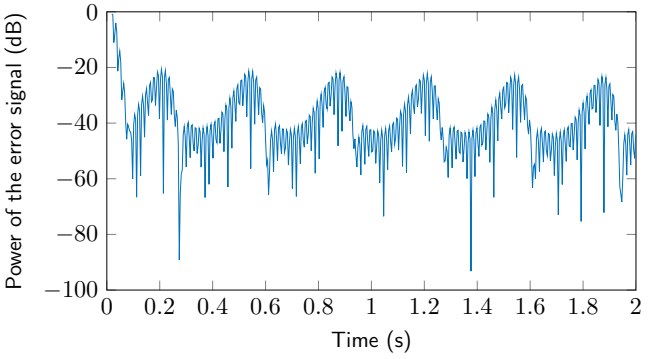

(c) Xiao's system when $\rho = 0.985$.

Figure 2.14: Comparison between Xiao's system and the traditional narrowband system. The signal $d(n)$ contains two pure sinusoids at $f_0 = 300Hz$ and $f_1 = 303Hz$, the step sizes are set to $\mu_0 = \mu_1 = 0.0015$ in all simulations, the pole-attraction factor in Xiao's system is set to two different values, the order of the secondary-path model is $L' = 150$ and the sampling frequency is $F_s = 8000Hz$.

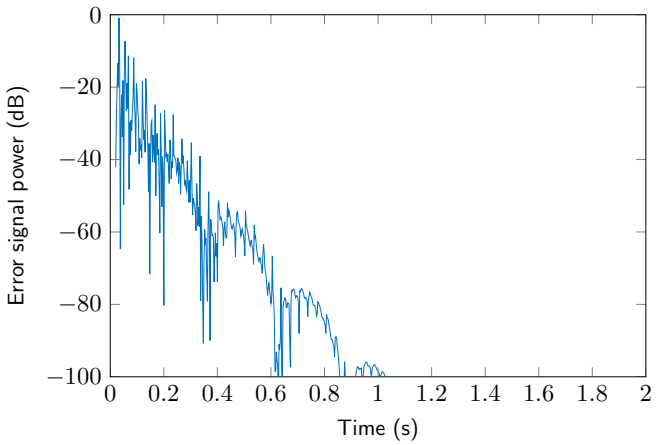

(a) Traditional system based on FxLMS.

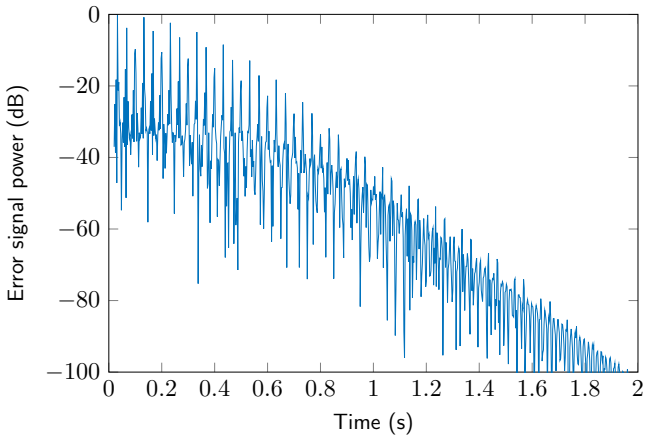

(b) Xiao's system when $\rho = 0.9999$.

Figure 2.15: Comparison between Xiao's system and the traditional narrowband system. Signal $d(n)$ contains $M = 20$ harmonics with fundamental $f_0 = 30Hz$, the order of the secondary-path model is $L' = 150$, the sampling frequency is $F_s = 8000Hz$ and the step sizes are employed in both simulations. If $\rho = 0.985$, Xiao's system is unstable because the bandpass filters are not sharp enough to separate the filtered reference signals. If $\rho = 0.9999$, the system is stable but it is still slower than the traditional system.

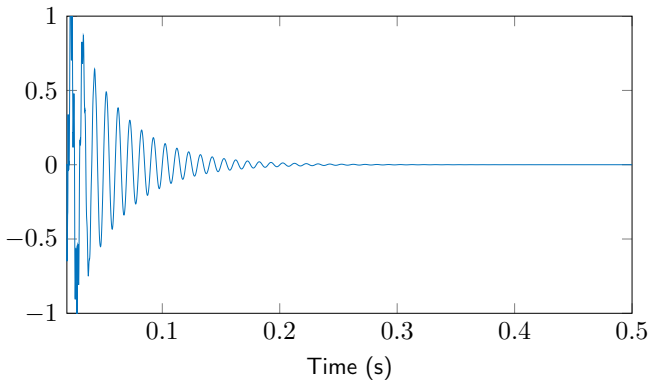

(a) $M = 1$, $\mu_0 = 0.2935$.

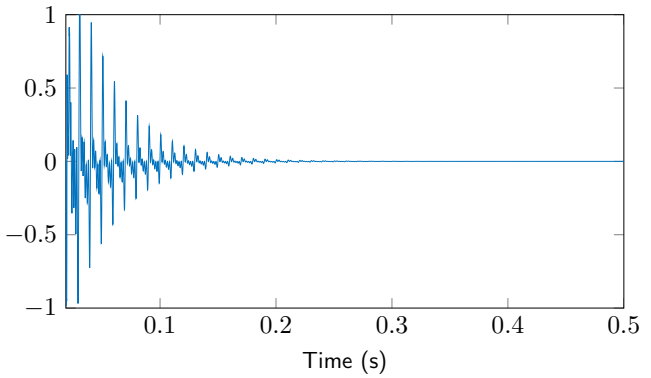

(b) $M = 5$, $\mu_0 = 0.2935$, $\mu_1 = 0.0188$, $\mu_2 = 0.0019$, $\mu_3 = 0.0008$ *and* $\mu_4 = 0.0004$.

Figure 2.16: The traditional system based on FxLMS is tested. In the first picture, only one harmonic $f_0 = 100Hz$ *is present. In the second picture,* $M = 5$ *harmonics are present with fundamental* $f_0 = 100Hz$ *and* $f_i = (i+1)f_0, i = 1, 2, 3, 4$. *Both pictures show the residual signal* $e(n)$. *The performance degradation when controlling one single frequency or five is not noticeable.*

bandpass filters. Furthermore, as shown in Figure 2.16, the degradation in convergence speed is limited in the parallel-form narrowband ANC system when multiple harmonics are being controlled. The performance degradation encountered when controlling multiple harmonics seems inevitable and the solutions proposed so far in the literature have not solved this problem.

2.5.1.3 Conclusions

In conclusion, both these solutions try to improve the performance of the traditional narrowband ANC architecture by introducing bandpass filters in the scheme. However, the traditional system still outperforms them in some situations. Xiao's system in particular, although certainly computationally more efficient than the traditional system, struggles to control sinusoidal interferences that are close in frequency and is very sensitive to the choice of the pole-attraction factor ρ.

2.5.2 The frequency estimation problem

2.5.2.1 A theoretical analysis of narrowband ANC in the presence of frequency mismatch

A 2010 paper [13] studied the effect of frequency mismatch on narrowband ANC and investigated the intricate interplay of several different parameters in determining the attenuation performance of the system:

Stability The stability bounds for both the step size and the secondary-path phase-estimation error are in substantial agreement with the 90° condition found in other ANC contexts.

Optimal step size To minimise the excess mean square error (MSE) in the presence of FM, an expression for the optimal step size is found.

Noise reduction The noise reduction (NR) is formulated in terms of the FM, the step size and the secondary-path phase error. As expected, the NR can be increased by reducing the FM and/or by increasing the step size. As the phase error increases though, the noise reduction may either increase or decrease depending on the sign of the FM.

2.5.2.2 Mitigation of the performance drop due to frequency mismatch

Various efforts have been recently carried out to provide more reliable frequency estimators to be integrated in narrowband ANC systems.

(a) In-ear. *(b) Supra-aural.* *(c) Circum-aural.*

Figure 2.17: Typical off-the-shelf commercial noise-cancelling headphones.

A 2004 paper [14] replaced the conventional hardware-based cosine wave generator with a software-based one; the information from the non-acoustic sensor is mapped to the frequency of the generated reference sinusoid through an AR-based filter, providing a way to reduce the FM with an LMS-like algorithm (which preserves the cost-efficiency of the conventional narrowband architecture). The new system provides improved robustness against frequency-estimation errors as large as 10%.

The minimum variance distortionless response (MVDR) spectral estimation was integrated in a conventional narrowband ANC system to minimise the FM in [15]. The iterative frequency-estimation algorithm based on the MVDR spectrum was chosen because of its accuracy and fast convergence, which improved the performance of the overall system. Theoretical analyses were also provided and verified through computer simulations with respect to FM, phase errors in secondary-path estimation and amplitude, phase and frequency variations of the sinusoidal interferences.

A new system was proposed in 2014 [16] that substituted the cosine generators used in conventional narrowband ANC systems with functional link artificial neural network (FLANN) units which provide superior performance even in the presence of 10% FM.

2.6 ANC applications

2.6.1 Headsets

Noise-cancelling headsets have been one of the most successful applications of ANC technology: while the first ANC headset was patented as early as

the 50s [17] [18], it was in 1989 that the first commercial noise-cancelling headphone was marketed by Bose inside a flight helmet. Throughout the 90s, other companies joined Bose in manufacturing ANC headsets mainly for military and civil aviation use. In 2000, Bose launched the Bose QuietComfort Headphone, the first consumer noise-cancelling headphone; since then, many companies (e.g. Sony, Sennheiser, etc) have marketed different models in a price range that spans entry-level products (just below a hundred euros), top-of-the-line consumer devices (several hundreds of euros) to high-end multi-purpose industrial or military headsets (several thousands of euros).

Many ANC techniques have been implemented on noise-cancelling headphones in the recent literature.

In 2002 [19] Gan and Kuo proposed a novel ANC headset design based on internal model control. While most research headsets at the time were based on adaptive feedforward technology and suffered from stability and performance deficiencies due to nonstationary reference inputs, spatially incoherent noise sources, acoustic feedback and practical constraints, they based their headset on adaptive feedback control.

The noise-control system was to be integrated into an existing audio playback system (such as an mp3 player) and could discriminate between the unwanted noise and the audio signal without degrading the latter. On top of that, the system tried to alleviate the instabilities due to changes in the secondary path by including online secondary-path modelling.

The system was improved in later articles [20] [21] by studying the optimal position of the microphone within the ear cup to obtain the flattest secondary-path magnitude response, since spectral flatness makes the algorithm less prone to instability. Secondly, by analysing the effects of modelling the secondary path using a generic audio signal instead of white noise, they discovered that music could have a threefold use: as a masking signal for residual noise using psychoacoustics principles [22] and as an excitation signal for both offline and online secondary-path estimation (as long as the piece of music is spectrally rich within the control frequency range).

Some extensions to this basic system have been in the direction of hybridising it with other systems [23] [24] [25] to make up for the shortcomings

of a pure feedback system, such as the difficulty of removing unpredictable broadband noise (e.g. white noise), possible feedback-loop instability and the absence of verifiable and strong theoretical results regarding algorithmic stability save for a few efforts in this direction [26] [27] [28]). Alternatively, cost-effective solutions [29] and alternative algorithms to the plain FxLMS [30] have been explored.

Other papers studied ways to solve the communication problem, i.e. discriminating between noise and useful signal in applications where communication is vital (e.g. flight helmets), since traditional broadband algorithms minimise the error signal completely [31] [32].

Finally, headset-specific approaches to dealing with secondary-path effects have been researched in order to find robust solutions to abrupt changes in the transfer function when the headphones are shifted around the ears or lifted entirely [33] [34] [24].

Other practical applications for ANC headsets explored in the recent literature include: a head-mounted ANC system with speech communication to deal with high-decibel magnetic resonance imaging (MRI) scanners [35], a feedforward audio-integrated ANC system for motorcycle helmets [36] and a hearing aid-integrated ANC headset for hearing-impaired industrial workers [37].

Chapter 3

The proposed system

The previous chapter discussed several variations of Widrow's adaptive notch filter that have been proposed in the ANC literature to control periodic noise.

In the 80s two different approaches for the compensation of the phase delays introduced by the secondary path were proposed.

In [2], the sinusoidal reference signals are convolved with an FIR estimate of the secondary path so that the FxLMS algorithm may be used to update the narrowband controller. This approach offers good noise attenuation and fast convergence time and it has been studied thoroughly in the literature. However, it suffers from the linearly increasing computational cost of convolving each reference signal with a high-order secondary-path estimate.

In [3], a phase lag Δ is estimated for each controlled frequency from a secondary-path model and the reference signals are delayed accordingly. The update algorithm for this system can be seen as a variation of the FxLMS algorithm where the secondary-path estimate is a frequency-dependent unit-delay block. This approach is computationally more efficient than the previous one, but it performs worse because the phase delay introduced by the $z^{-\Delta}$ block is different in general from the phase delay actually introduced by the secondary path.

In recent years, two variations of the traditional narrowband ANC system based on FxLMS have been proposed to improve it.

In [4], Xiao proposed a system that only requires one single convolution

per iteration regardless of the number of controlled harmonics; while very computationally efficient, the system's performance suffers from the introduction of a bank of bandpass filters when close frequencies must be controlled and the system is very reliant on the correct choice of a bandwidth-control parameter to separate the filtered reference signals.

In [11] Chang and Kuo developed a parallel narrowband ANC system that uses bandpassed individual error signals to update the corresponding controllers instead of a single error signal as in the traditional narrowband system. However, this modification does not always yield better convergence time than the traditional system (as discussed in [12]) because of an overlooked issue in the design of the bandpass filterbank.

Thus, Xiao's and Ziegler's systems are computationally more efficient than the traditional system but they encounter performance issues in several situations.

Furthermore, all these systems suffer from two additional problems if they are extended to parallel multi-harmonic control and online modelling of the secondary path. Firstly, the parallel approach these systems use to control multiple harmonics allows each harmonic to be controlled independently with a different step size, but, since tuning each step size manually is difficult, these systems often implement the normalised FxLMS algorithm, which increases the computational cost linearly with the number of controlled harmonics. Secondly, all the systems are slow in reacting to changes in the secondary path because the high order of the secondary-path estimate requires a small online-adaptation step size.

The system we propose reduces the convolutional cost of the conventional system by employing lower-order FIR models of the secondary path called *local secondary paths* and at the same time it maintains roughly the same performance properties; additionally, the proposed system offers faster online adaptation to changes in the secondary path thanks to the low order of the *local secondary paths* and it offers cost-effective independent control of each harmonic component with an empirical step size-correction law.

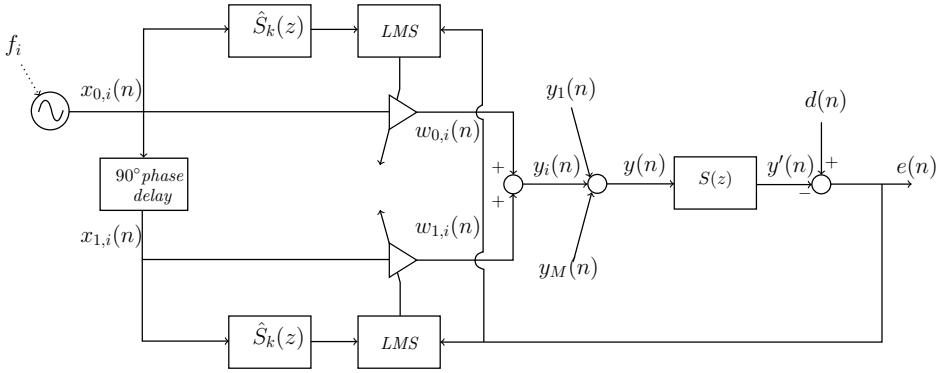

Figure 3.1: The proposed system employs a local estimate of the secondary path.

3.1 Local secondary paths

To reduce the computational cost of the reference-filtering operations, our idea is to substitute the *global* L'-order secondary-path estimate $\hat{S}(z)$ that has been used so far in the literature with a set of *local* L-order secondary-path estimates $\hat{S}_k(z)$ (Figure 3.1). Local secondary-path estimates are FIR filters that approximate the secondary path well enough in a neighbourhood of a certain frequency f_k.

The order L' of the global estimate $\hat{S}(z)$ must be quite large in order to provide a decent spectral approximation of $S(z)$ over the whole control frequency range. However, convolving a tonal reference signal with $\hat{S}(z)$ essentially only yields a phase-shifted and amplified version of the input sinusoid. For this reason, to control one known frequency we only need two parameters to obtain the filtered reference signals: the phase and the magnitude of $S(z)$ at that frequency. For example, Ziegler's narrowband ANC system uses a pure-delay unit to compensate for the delay introduced by the secondary path, which can be interpreted as an *ultra-local* secondary-path approximation (even though the amplitude is not taken into account and the integer delay compensation is not accurate in practice).

We here propose a different approach: after splitting the frequency axis into K frequency bins of width Δf from the lowest frequency f_L to the largest frequency f_H such that

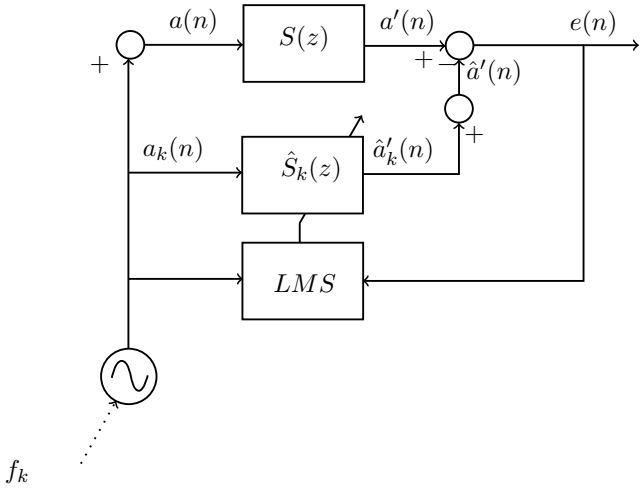

Figure 3.2: Offline modelling using sinusoidal excitation signals. This scheme is equivalent to the one in Figure 3.4 when the ANC controllers are switched off.

$$K = \frac{f_H - f_L}{\Delta f}, \tag{3.1}$$

the offline-modelling system (as shown in Figure 3.2) feeds the cancelling loudspeaker the sum of the sinusoidal excitation tones

$$a_k(n) = \overline{\delta}\cos(2\pi f_k n) \qquad k = 0,\ 1,\ \ldots,\ K-1 \tag{3.2}$$

at the *central frequency* f_k of the k-th bin

$$f_k = \frac{2f_L + \Delta f(2k+1)}{2} \qquad k = 0,\ 1,\ \ldots\ K-1. \tag{3.3}$$

The signal that is picked up by the error microphone is the convolution between the sinusoidal excitation signals and the (infinite) secondary-path impulse response $s(n)$:

$$a'(n) = (a * s)(n) = \left(\sum_{k=0}^{K-1} a_k * s\right)(n). \tag{3.4}$$

Each controller produces the signal

$$\hat{a}'_k(n) = \sum_{l=0}^{L-1} \hat{s}_l(n) a_k(n-l) \qquad k = 0,\ 1,\ \ldots,\ K-1, \tag{3.5}$$

subtracts it from the error-microphone signal $a'(n)$

$$e(n) = a'(n) - \hat{a}'(n) = a'(n) - \sum_{k=0}^{K-1} \hat{a}'_k(n) \tag{3.6}$$

and finally adjusts its local secondary-path estimate according to the FxLMS algorithm

$$\hat{\mathbf{s}}_\mathbf{k}(n+1) = \hat{\mathbf{s}}_\mathbf{k}(n) + \mu_s \mathbf{a}_\mathbf{k}(n) e(n) \qquad k = 0,\ 1,\ \ldots,\ K-1 \tag{3.7}$$

where

- $\hat{\mathbf{s}}_\mathbf{k}(n) = [\hat{s}_{k,0}(n)\ \hat{s}_{k,1}(n)\ \ldots\ \hat{s}_{k,L-1}(n)]^T$ is the impulse response of the local L-order secondary-path estimate $\hat{S}_k(z)$,
- $\mathbf{a}_\mathbf{k}(n) = [a_k(n)\ a_k(n-1)\ \ldots\ a_k(n-L+1)]^T$ is the excitation-signal vector and
- μ_s is the offline-modelling step size.

In the z-transform domain, we have that

$$A'(z) = S(z)A(z) = S(z) \sum_{k=0}^{K-1} A_k(z) \tag{3.8a}$$

$$\hat{A}'(z) = \sum_{k=0}^{K-1} A'_k(z) = \sum_{k=0}^{K-1} \hat{S}_k(z) A_k(z) \tag{3.8b}$$

so that $E(z)$ becomes

$$\begin{aligned} E(z) = A'(z) - \hat{A}'(z) &= \sum_{k=0}^{K-1} S(z)A_k(z) - \sum_{k=0}^{K-1} \hat{S}_k(z)A_k(z) = \\ &= \sum_{k=0}^{K-1} \left(S(z) - \hat{S}_k(z) \right) A_k(z). \end{aligned} \tag{3.9}$$

Therefore, the minimum for the k-th optimisation problem is reached when

$$\hat{S}_k(z) \equiv S(z) \tag{3.10}$$

in correspondence of the central frequencies f_k.

After convergence, each local secondary path $\hat{S}_k(z)$ will yield a good local approximation in a Δf-wide neighbourhood of f_k by virtue of the fact that the magnitude and phase of the secondary path at frequency f_k will be identified accurately. However, since the offline-modelling signal only excites $S(z)$ at the central frequency, the approximation for near frequencies within the frequency bin will not be as accurate, depending on the order L of $\hat{S}_k(z)$ and the frequency-bin width Δf, as shown in Figure 4.2. This is a small price to pay for the advantages the local-identification approach brings, but simulations prove that this (tunable and controllable) inaccuracy does not noticeably slow down the convergence speed thanks to the robustness of Widrow's adaptive notch filter to identification errors. The only care that must be taken is to design Δf and L so that the frequency bins are narrow enough to ensure stability (in other words, the phase error should remain well below 90° within the frequency bin).

As a further remark, it should be noted that the primary noise $d(n)$ (if present during the offline-modelling phase) and every other excitation signal $a_i(n)$ $(i \neq k)$ act as disturbances for the identification of a given local secondary-path model $\hat{S}_k(z)$. If this turns out to be an issue, each local model may be learnt separately at the cost of a longer offline-modelling time. However, simulations show that modelling the local transfer functions simultaneously does not put a strain on the system and each local model converges to a good solution after a reasonable time.

Once the local secondary paths $\hat{S}_k(z)$ have converged, the narrowband ANC units in Figure 3.1 can be switched on. Each sinusoidal reference signal $x_{0,i}(n)$ and $x_{1,i}(n)$ is convolved with the local secondary path $\hat{S}_k(z)$ its frequency falls under:

$$k : f_i \in \left(f_k - \frac{\Delta f}{2}; f_k + \frac{\Delta f}{2} \right]. \tag{3.11}$$

The local-modelling approach here proposed can be seen as a compromise between the *frequency-wise* modelling used by Ziegler and the *global*

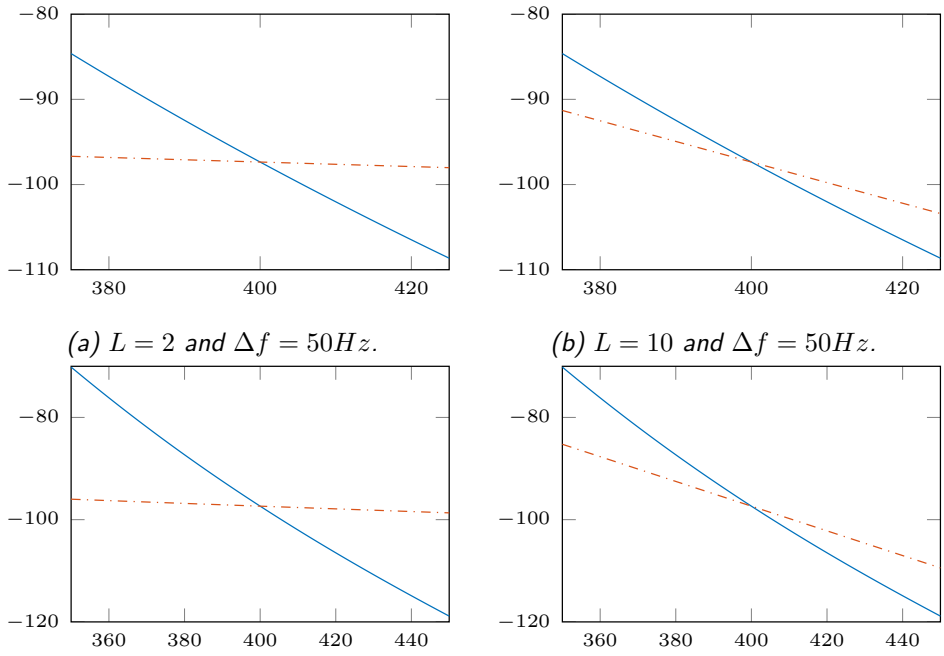

(a) $L = 2$ *and* $\Delta f = 50Hz$. *(b)* $L = 10$ *and* $\Delta f = 50Hz$.

(c) $L = 2$ *and* $\Delta f = 100Hz$. *(d)* $L = 10$ *and* $\Delta f = 100Hz$.

Figure 3.3: The solid line depicts the secondary-path phase response while the dash-dotted line is the estimated phase by the local model; as expected, the transfer functions intersect at the central frequency $400Hz$ *and provide a decent approximation in a* Δf*-wide neighbourhood. The largest phase-estimation error within the frequency bin varies depending on* L *and* $\Delta f = 100Hz$.

modelling of the traditional narrowband FxLMS algorithm. The advantage with respect to the global-identification approach lies in the reduced computational burden. Instead of convolving the reference sinusoids $x_0(n)$ and $x_1(n)$ with a long FIR model $\hat{S}_k(z)$, as few as two coefficients can be sufficient to provide a decent local approximation, provided that the frequency bins are small enough. The proposed system also achieves better performance with respect to Ziegler's system, since the provided estimation error is lower. Moreover, estimating Ziegler's delay requires the computation of the discrete Fourier transform of $\hat{S}(z)$ and of its group delay which may prove to be computationally demanding when the controlled frequency changes and the system must be able to provide a phase lag Δ for each frequency in the control frequency range $[f_L, f_H]$.

Two final comparative remarks:

- If we imagine to have infinitesimal frequency bins ($\Delta f \to 0$) and thus an infinity of sinusoidal excitation signals spanning the entire control frequency range, the local-identification approach becomes equivalent to the global-identification approach from a spectral viewpoint.

- In practice, the phase lag Δ in Ziegler's system must be integer, which implies that multiple frequencies will be assigned to the same phase lag. Similarly in our approach a group of adjacent frequencies is assigned to the same local secondary-path estimate. However, instead of a pure-delay unit, the proposed system uses an L-order FIR filter, which is more accurate.

3.1.1 On the excitation signals

The system we propose employs sinusoidal excitation signals in order to estimate the low-order local secondary paths. This method yields minimal spectral overlapping between the excitation signals and allows as few as two coefficients to be used in estimating the local models. Spectral overlapping between the excitation signals determines a degradation in convergence time because the signals will interfere with each other's local identification, since a single error signal is used to adapt the local models.

Nonetheless, other approaches to the estimation of the local secondary paths may be explored. We will present two possible excitation signals that may be used for this purpose. Choosing the excitation signal presents a tradeoff between model order, which determines the convergence time of the offline and online modelling processes, and estimation accuracy, which determines the performance of the narrowband ANC units that employ those local models to compensate the secondary-path effects.

3.1.1.1 Bandpassed white noise

Bandpassed white noise might be employed as the excitation signal:

$$a_k(n) = (w_k * h_k)(n) \qquad k = 0,\ 1,\ \ldots,\ K-1 \tag{3.12}$$

where $w_k(n)$ is a zero-mean white-noise signal with variance $\sigma^2_{w_k}$

$$w_k(n) \sim W.N.(0, \sigma^2_{w_k}) \qquad k = 0,\ 1,\ \ldots,\ K-1 \tag{3.13}$$

and $h_k(n)$ is the impulse response of a bandpass filter $H_k(z)$. The bandwidth of each bandpass filter must be centred at the central frequency f_k (Equation 3.11) of the k-th frequency bin and the quality factor must be designed so that the spectral overlapping is small outside the frequency bin in order to reduce the interference between the excitation signals.

Employing bandpassed white noise as the excitation signal yields more accurate local models with respect to the single-sinusoid approach, but it requires higher-order local secondary paths, which increase the computational cost associated to the reference-filtering operations. Furthermore, the spectra of the bandpassed white-noise signals always overlap to some extent, which slows down the convergence of the offline and online modelling process.

3.1.1.2 Multiple sinusoids

Since using a single sinusoid at the central frequency f_k of each frequency bins allows the local secondary paths to only model the secondary path accurately at f_k, we can use multiple excitation sinusoids within the k-th frequency bin so that the k-th local model will interpolate the secondary path between these frequencies and be more accurate. This can be interpreted as a generalisation of the single-sinusoid approach.

The excitation signals become

$$a_k(n) = \sum_{i=0}^{N-1} \overline{\delta}_i \cos(2\pi\phi_{k,i} n) \qquad k = 0,\ 1,\ \ldots,\ K-1, \tag{3.14}$$

where the N frequencies $\phi_{k,i}$ belong to the k-th frequency bin. For example, if $N = 2$, the two excitation frequencies may be chosen as

$$\phi_{k,0} = f_k - \frac{\Delta f}{2} \tag{3.15a}$$

$$\phi_{k,1} = f_k + \frac{\Delta f}{2} \tag{3.15b}$$

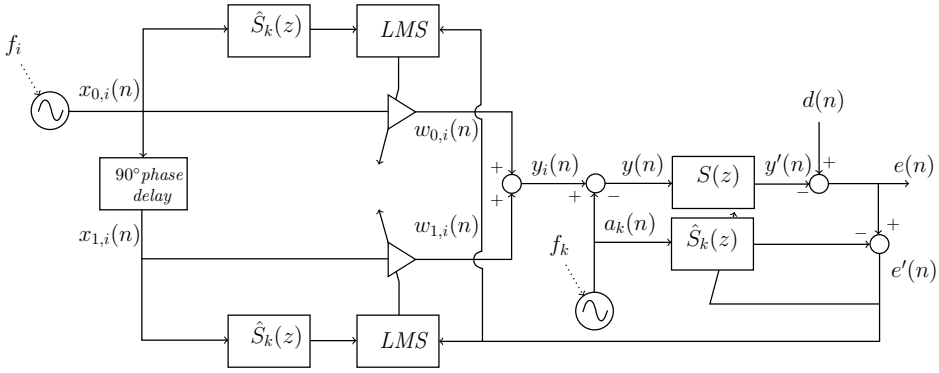

Figure 3.4: The proposed system, with online modelling and multiple narrowband controllers arranged in parallel. Only one controller and one online-modelling unit are shown for convenience.

and when $N = 1$ we have the single-sinusoid approach:

$$\phi_{k,0} = f_k. \tag{3.16}$$

This approach yields more accurate models as N increases. However, higher order models will be needed, which deteriorates the convergence time of the offline and online modelling systems, and a large number of excitation sinusoids might degrade the performance of the ANC units.

3.2 Online modelling of local secondary paths

In order to adapt to a time-varying secondary path, the K online-modelling units in Figure 3.4 adapt to changes in the secondary path by injecting the system with small-amplitude sinusoids at the central frequency f_k (Equation 3.11) of each frequency bin (Equation 3.2) and they use the FxLMS algorithm (Equation 3.7) to update the filter weights of each local secondary path $\hat{S}_k(z)$. If we turn off the ANC units, the system is equivalent to the one in Figure 3.2 and thus can perform offline modelling.

The amplitude $\overline{\delta}$ of the online-modelling excitation signals must be designed with special care because it determines the system reactivity to changes in the secondary path but at the same time it determines the achievable level of noise attenuation since it is injected at the control point. More-

over, when the local models are converging after a change in the secondary path, the sinusoids act as a disturbance for the narrowband controllers. Consequently, a tradeoff between reactivity and noise reduction must be resolved in practice when implementing the online-modelling subsystem.

In the z-transform domain, the expression for $e'(n)$ becomes

$$E'(z) = D(z) - \sum_{i=0}^{M-1} S(z)Y_i(z) + \sum_{k=0}^{K-1} \left(S(z) - \hat{S}_k(z)\right) A_k(z) \tag{3.17}$$

which can be approximated to

$$E'(z) \approx D(z) - \sum_{i=0}^{M-1} S(z)Y_i(z) \tag{3.18}$$

when the local secondary paths have converged to their optimal solution. Therefore, $e'(n)$ may be used to update the ANC units as well as the local secondary-path estimates.

The reactivity of the system to changes in the secondary path depends on the step size μ_s (see Equation 3.7) and the amplitude of the excitation signals $\overline{\delta}$. While the second should be kept as small as possible for the reasons outlined above, the first can be designed to speed up the algorithm within the limits of stability.

Since the stability condition of the FxLMS algorithm is determined by the order of the adaptive filter, the low-order filters used to estimate the secondary path allow great reactivity to changes in the secondary path. Instead, systems with online modelling of a global transfer function adapt to changes more slowly because the upper limit for the online-modelling step size is lower. This can become dangerous when the phase difference between the secondary-path model and the secondary path exceeds 90° and the online-modelling subsystem fails to keep track of the change.

An alternative solution to compensate for the small amplitude of the online-modelling excitation sinusoids is to use the normalised version of the FxLMS algorithm:

$$\hat{\mathbf{s}}_\mathbf{k}(n+1) = \hat{\mathbf{s}}_\mathbf{k}(n) + \frac{\mu_s \mathbf{a_k}(n) e'(n)}{\mathbf{a_k}^T \mathbf{a_k} + \epsilon} \qquad k = 0,\ 1,\ \ldots,\ K-1 \tag{3.19}$$

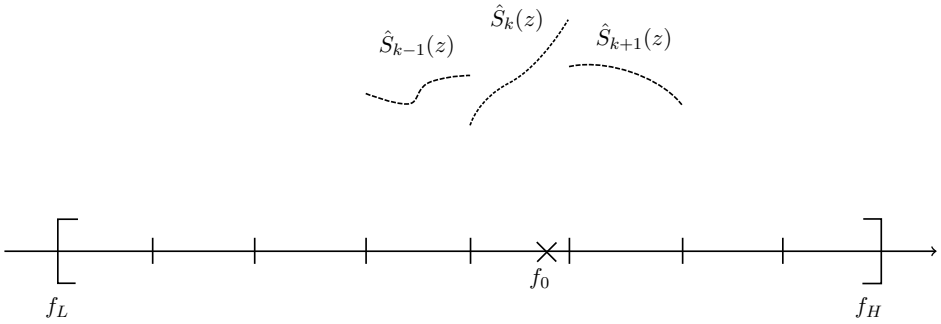

Figure 3.5: In this case, the system is only controlling one frequency f_0, which belongs to the k-th frequency bin. Therefore, the online-modelling subsystem only models $\hat{S}_k(z)$ and its two adjacent estimates $\hat{S}_{k-1}(z)$ and $\hat{S}_{k+1}(z)$.

where ϵ is a tunable regularisation term to avoid instability when $\hat{\mathbf{a}}_\mathbf{k}(n) \equiv 0$ and μ_s is the normalised step size. This approach requires more computations per iteration but it is less reliant on the proper choice for the step size.

3.2.1 An efficient modification

In general the undesired harmonics f_i may not always occupy every frequency bin (i.e. there may exist a frequency bin k that is currently being unused by the ANC units). If this is the case, the system does not need to update the local secondary paths to which no controlled frequency is associated. Instead, it may decide to adapt only the local models that are actually being used by some ANC unit.

The advantages of this modification are twofold. First, the computational cost due to the online modelling is reduced. Secondly, since fewer online-modelling excitation signals will be injected into the system at the control zone, the noise-attenuation degradation due to their presence is reduced. If the controlled frequencies are time varying, we might want to also model the two adjacent frequency bins to each currently used local model in order to have a safety margin should the controlled frequency change and fall under another frequency bin (Figure 3.5).

3.3 Empirical step size-correction law

In parallel-form narrowband ANC systems, each secondary-path convolution has the effect of scaling each step size μ_i by the magnitude value of the secondary path at the controlled frequency f_i. In fact, the FxLMS update rule for the first coefficient becomes

$$\begin{aligned} w_{0,i}(n+1) &= w_{0,i}(n) + \mu_i x'_{0,i}(n)e(n) = \\ &= w_{0,i}(n) + \mu_i A_{\hat{S}_k} A\cos(2\pi f_i n + \Phi_{\hat{S}_k})e(n) \\ &\quad i = 0,\ \ldots,\ M-1 \end{aligned} \tag{3.20}$$

where $A_{\hat{S}_k} = \left|\hat{S}_k(e^{j2\pi f_i})\right|$ and $\Phi_{\hat{S}_k} = \angle\hat{S}_k(e^{j2\pi f_i})$ and similarly for the second coefficient. Let us remind that by reducing the step size the convergence slows down and conversely by increasing the step size the convergence speeds up.

Since in practice it is impossible to tune each step size manually to compensate the scaling and force comparable convergence times on the controllers, to this end we propose the following empirical step size-correction law:

$$\mu_i = \frac{\alpha}{\left|\hat{S}(e^{j2\pi f_i})\right|^{\beta}} \qquad i = 0,\ \ldots,\ M-1, \tag{3.21}$$

where α and β are two tunable parameters ($\alpha = \beta = 1$ for example). A more efficient alternative to computing $\left|\hat{S}(e^{j2\pi f_i})\right|$ for each possible controlled frequency could be to compute a representative magnitude value for each frequency bin after offline secondary-path identification so that the μ-correction law becomes

$$\mu_i = \frac{\alpha}{A_i^{\beta}} \qquad i = 0,\ \ldots,\ M-1, \tag{3.22}$$

where A_i can be, e.g.:

- The average magnitude of the local secondary-path model over the frequency bin.

- The maximum magnitude within the frequency bin for a more conservative solution (for what concerns stability).

This step size-correction law is equivalent to the normalised version of the FxLMS algorithm, whose update law (in the single-frequency case) becomes

$$w_j(n+1) = w_j(n) + \frac{\mu x'_j(n) e(n)}{x'_j(n)^2} \qquad j = 0,\ 1. \tag{3.23}$$

In fact, dividing by the square of $x'_j(n)$ is equivalent to scaling by the reciprocal of the squared magnitude of $\hat{S}_k(z)$. However, instead of performing the normalisation at every iteration, μ correction is performed only once (or until the controlled frequency changes).

3.4 Characteristics of the proposed system

We conclude this chapter with a brief summary of the characteristics and relative advantages of the system introduced in the preceding sections:

Local secondary paths Switching from high-order global secondary-path estimates to lower-order local models allows the system to perform fewer multiplications and additions per iteration. Furthermore, these local models allow the system to be very reactive to secondary-path changes during the operations of the system. The downside of estimating local models with sinusoidal excitation signals however is that the approximation may become too rough and particular care must be taken in designing their "range of validity" (here defined as frequency-bin width) so that the models satisfy the 90° stability condition. This notwithstanding, the adaptive notch filter our system is based on is very robust to estimation errors and exhibits good performance even in the presence of estimation errors.

Independent control of harmonics with step size correction Each modified ANC controller can choose its own step size independently according to the μ-correction formula that acts as a normalisation term for the FxLMS algorithm. This is especially important in case of frequency mismatch when the secondary path attenuates some control

frequency, since a larger step size widens the rejection bandwidth of the adaptive notch filter.

Chapter 4

Computer simulations

In this chapter computer simulations are carried out in MATLAB to assess the performance of the proposed narrowband ANC system with respect to three other systems presented in the previous chapters: the traditional narrowband ANC system [2], Ziegler's system [3] and Xiao's system [4].

Two types of noise are used:

Synthesised noise A sum of sinusoids was used to give a first evaluation of the performance of the systems. Synthesising the noise gives us a good degree of flexibility in testing the systems against a wide range of different scenarios (multiple frequencies, mixture of sines and wideband noise, varying frequencies, etc).

Recorded noise A recording of a motorbike engine was used to assess the robustness of the systems to real-life harmonic noises, whose frequencies tend to flicker to some extent and which normally come embedded in wideband noise or other signals (e.g. speech).

We simulated the secondary path $S(z)$ using a compact 24th-order infinite impulse response (IIR) filter with 24 poles and 24 zeros. Its frequency response is shown in Figure 4.1a and its zero-pole plot is shown in Figure 4.1b. Using an IIR filter instead of a finite impulse response (FIR) filter to simulate the secondary path yields more realistic simulation results. The secondary path was taken from the textbook "Active Noise Control Systems: Algorithms and DSP Implementations" [6].

The sampling frequency is $F_s = 8000Hz$ in all simulations and the control frequency ranges from $f_L = 0Hz$ to $f_H = 700Hz$. This choice is somewhat arbitrary in a simulated context and the range was decided to be in line with the range of frequencies that real active noise control systems are normally able to control. Furthermore, since the highest controlled frequency is much lower than the Nyquist frequency, any potential effect on the system noise-attenuation capabilities when the controlled frequencies approach $\frac{F_s}{2}$ will not be present.

4.1 Local secondary paths

In this section, we first provide a computational analysis to estimate the reduction in computational cost that the proposed system allows with respect to the conventional system based on global modelling. We provide a spectral comparison between the IIR secondary path $S(z)$, the global secondary-path estimate $\hat{S}(z)$ used in traditional narrowband ANC systems and the local secondary-path estimates $\hat{S}_k(z)$ used in our system. Finally, we carry out some representative simulations to verify that our system achieves comparable noise-cancellation and convergence-speed results with respect to the traditional narrowband ANC system and that it performs better than Xiao's and Ziegler's systems in some situations.

4.1.1 Computational analysis

The conventional narrowband ANC system compensates the phase delays and magnitude changes introduced by the secondary path by convolving each reference sinusoid with a global FIR estimate of the secondary path $\hat{S}(z)$, whose order L' must be quite large to provide a good spectral approximation of $S(z)$. The system we propose, instead, convolves each reference signal with a local L-order FIR estimate (i.e. an estimate that only has local validity within a certain frequency bin) $\hat{S}_k(z)$, whose order can be very low with respect to the global estimate. This reduces the cost of the ANC system for two reasons:

Space The memory needed to store the coefficients of the secondary-path

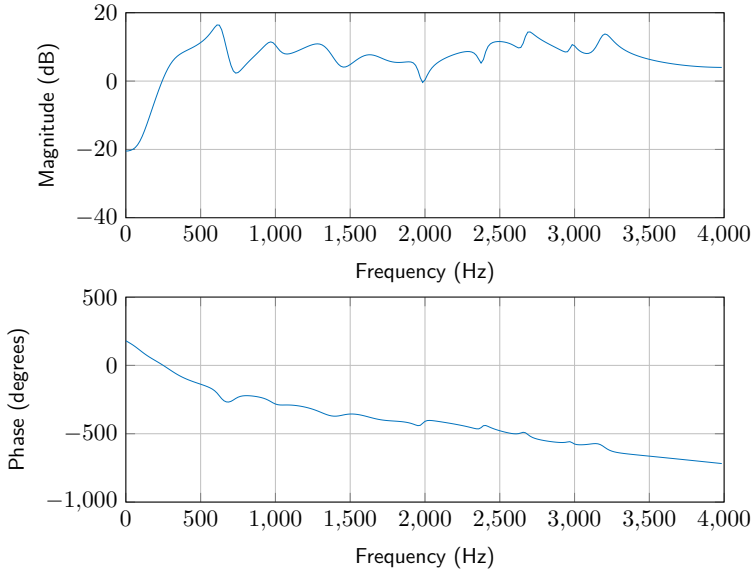

(a) Frequency response.

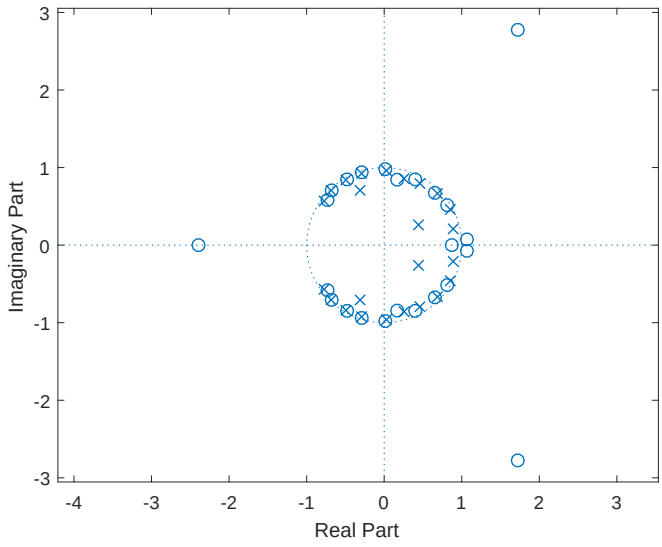

(b) Pole and zero plot.

Figure 4.1: The secondary path used in the simulations.

K \ L	2	5	10
7	14	35	70
14	28	70	140
21	42	105	210

Table 4.1: The memory needed to store the local secondary paths as a function of the number of local models K and their order L.

models is smaller.

Time The convolution operation requires fewer multiplications and sums.

4.1.1.1 Space

The storage space needed for the local secondary paths is proportional to LK, where $K = \frac{f_H - f_L}{\Delta f}$ is the number of frequency bins, whereas the memory needed to store the global secondary-path estimate is proportional to L'. As shown in Table 4.1, depending on the situation, as few as 14 total coefficients may need to be stored in the proposed system, which is one order of magnitude lower than the typical number of coefficients needed for an accurate global estimate.

4.1.1.2 Time

Table 4.2 compares the number of multiplications needed to obtain the filtered reference signals in the traditional system and in the proposed system when the orders of the secondary-path estimates (L and L') and the number of controlled harmonics (M) change. The convolution operation requires ML' multiplications per iteration in the traditional system and ML multiplications per iteration in the proposed system. The values for L and L' are some of the values we used when simulating the systems and they yield different degrees of accuracy (the higher the order, the more accurate the model).

The number of multiplications performed in the proposed system is reduced by a factor of $\frac{ML'}{ML} = \frac{L'}{L}$ with respect to the traditional system. In

M \ L'	100	150	200
1	100	150	200
5	500	750	1000
10	1000	1500	2000
20	2000	3000	4000

(a) The traditional system employs an estimate $\hat{S}(z)$ of order L'.

M \ L	2	5	10
1	2	5	10
5	10	25	50
10	20	50	100
20	40	100	200

(b) The proposed system employs several estimates $\hat{S}_k(z)$ of order L.

Table 4.2: The number of multiplications per iteration needed to convolve the reference signals as a function of the number of controlled harmonics M and the order of the secondary-path estimates L and L'.

our simulations, $L' = 150$ and $L = 5$ yield the same noise attenuation and speed of convergence, which means that the proposed system reduces the number of performed multiplications by a factor of $\frac{L'}{L} = \frac{150}{5} = 30$.

A new system was recently proposed in [4] by Xiao to reduce the computational cost of the conventional system. In this system, the reference signals are summed, their sum is convolved with a global estimate $\hat{S}(z)$ and each filtered reference signal is retrieved by filtering the convolved signal through a bank of bandpass filters. Xiao's system performs only L' multiplications per iteration regardless of the number of controlled harmonics and $4M$ multiplications due to the 3rd-order bandpass IIR filters

$$H_{bp,i} = \frac{(\rho - 1)c_i z^{-1} + (\rho^2 - 1)z^{-2}}{1 + \rho c_i z^{-1} + \rho^2 z^{-2}} \qquad i = 0,\ 1,\ \ldots\ M - 1, \tag{4.1}$$

where $c_i = -2\cos(2\pi f_i)$ and ρ is a pole-attraction factor that determines the bandwidth of the filter and the time constant associated to it.

Even though they vary depending on the number of controlled harmonics and secondary-path model orders, the number of multiplications performed by the proposed system and Xiao's system remain in the same order of magnitude:

- If $L = 10$, $L' = 100$ and $M = 20$, Xiao's system performs fewer multiplications than the proposed system: $L' + 4M = 180$ against $ML = 200$.

- However, if $L = 5$, $L' = 150$ and $M = 20$, the proposed system requires fewer multiplications per iteration: $L' + 4M = 230$ against $ML = 100$.

Finally, Ziegler's system is the most efficient of the four, since the delay blocks produce the filtered reference signals with zero multiplications. The system however has a significant offline overhead because it must compute the phase lags Δ for all possible controlled frequencies, which requires the computation of the discrete Fourier transform of $\hat{S}(z)$ and of its phase delay.

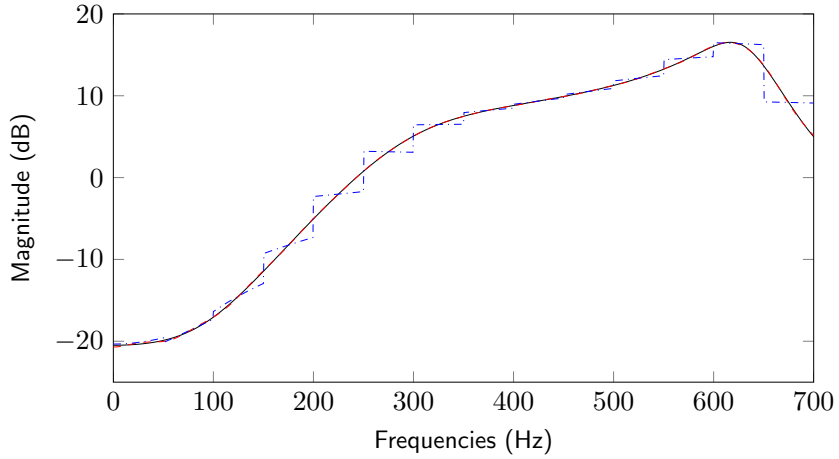

(a) Magnitude response.

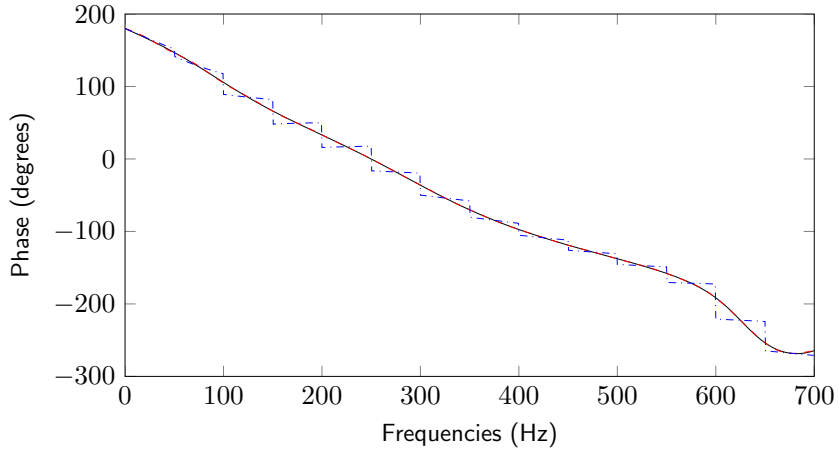

(b) Phase response.

Figure 4.2: Identification comparison between $S(z)$ (black solid line), $\hat{S}(z)$ (red dashed line) and $\hat{S}_k(z)$ (blue dash-dotted line).

4.1.2 Identification comparison between local and global estimates

Figure 4.2 shows the comparison between the frequency response of the secondary path $S(z)$, the global estimate $\hat{S}(z)$ and the local estimates $\hat{S}_k(z)$.

The secondary path is a 24th order IIR transfer function. The order of the global secondary-path estimate is $L' = 150$. The order of the $K = 14$ local secondary paths is $L' = 5$ and the width of the frequency bins is $\Delta f = 50Hz$. In order to estimate the local secondary paths we used the single-sinusoid approach.

The global estimate exhibits very good identification accuracy in the whole control frequency range, whereas the local secondary paths identify the secondary path accurately only at the central frequency of each frequency bin and exhibit various degrees of accuracy within the different frequency bins. For example, in the 9th frequency bin (between $400Hz$ to $450Hz$) the magnitude estimation provided by the local secondary path $\hat{S}_9(z)$ is comparable to that of $\hat{S}(z)$; in the 14th frequency bin (between $650Hz$ to $700Hz$) instead, $\hat{S}_{14}(z)$ yields a maximum $4dB$ magnitude-estimation error. In the first frequency bin (between $0Hz$ to $50Hz$), $\hat{S}_1(z)$ yields a maximum 5° phase-estimation error; in the 13th frequency bin (between $600Hz$ to $650Hz$) instead, the maximum phase-estimation error is 30°.

4.1.3 Identification comparison between local estimates with different excitation signals

In the previous chapter we discussed different approaches for the identification of the local models.

Figures 4.3 and 4.4 show the comparison between the identification accuracy yielded by two approaches. In the first case, the local secondary paths are learnt with a single excitation sinusoid centred at the central frequency of each frequency bin. In the second case, the local secondary paths are learnt with two excitation sinusoids positioned around the central frequency of each frequency bin. In the third case, the local secondary paths are learnt with a single bandpassed white-noise signal centred at the central frequency of each frequency bin.

In Figure 4.3, the excitation signals contain a single sinusoid at frequency $\phi_{k,0} = f_k$, the width of the frequency bins is set to $\Delta f = 50Hz$ and the order of the local models is $L = 5$. This results in $K = 14$ local secondary paths.

In Figure 4.4,the excitation signals contain a two sinusoids at frequencies $\phi_{k,0} = f_k - \frac{\Delta f}{2}$ and $\phi_{k,1} = f_k + \frac{\Delta f}{2}$, the width of the frequency bins is set to $\Delta f = 100Hz$ and the order of the local models is $L = 30$. This results in $K = 7$ local secondary paths.

The single-sinusoid approach is less accurate with respect to the two-sinusoid approach because the local models intersect the secondary path only at f_k, but it allows low-order local models. On the other hand, the approach with two sinusoids yields more accurate models that interpolate the secondary path in two points, but it requires a higher order. In practice, a tradeoff must be resolved between identification accuracy, which determines the noise reduction and convergence time, and model order, which determines the computational efficiency of the system and its reactivity to changes in the secondary path.

Another problem that may arise when designing the excitation signal for the local secondary path is spectral overlapping. In the sinusoid-based approaches exposed above, there is no spectral overlapping between the excitation signals. Instead, if bandpassed white noise is employed as the excitation signal, spectral overlapping is inevitable and it may degrade the identification accuracy. In Figure 4.5, the excitation signal contains bandpassed white noise centred at frequencies $\phi_{k,0} = f_k$, the width of the frequency bins is set to $\Delta f = 100Hz$ and the order of the local models is $L = 35$. Almost all local models are estimated accurately, but the first local estimate $\hat{S}_1(z)$ is not. This inaccuracy is due to the bias introduced by the spectral overlapping and it would determine instability in the system because the phase error exceeds the stability condition.

4.1.3.1 Effect on control

Figure 4.6 compares the performance of the three local-estimation approaches described above with respect to the performance of global estimates. The signal $d(n)$ contains one single sinusoid at $f_0 = 400Hz$ and the step size is

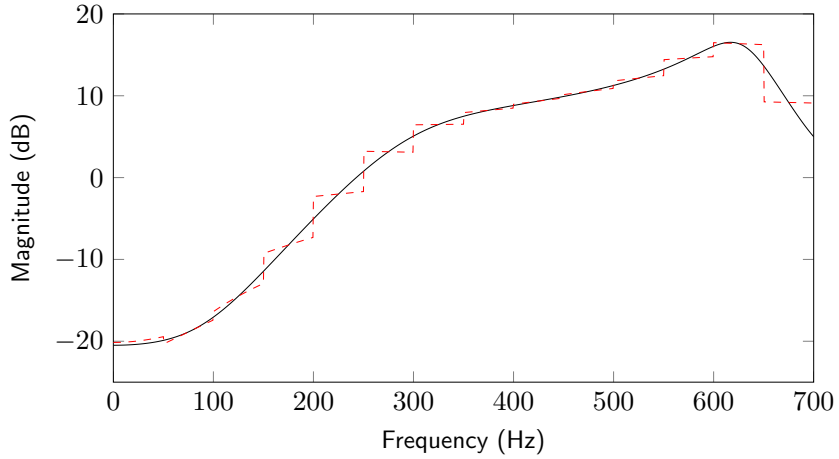

(a) Magnitude response.

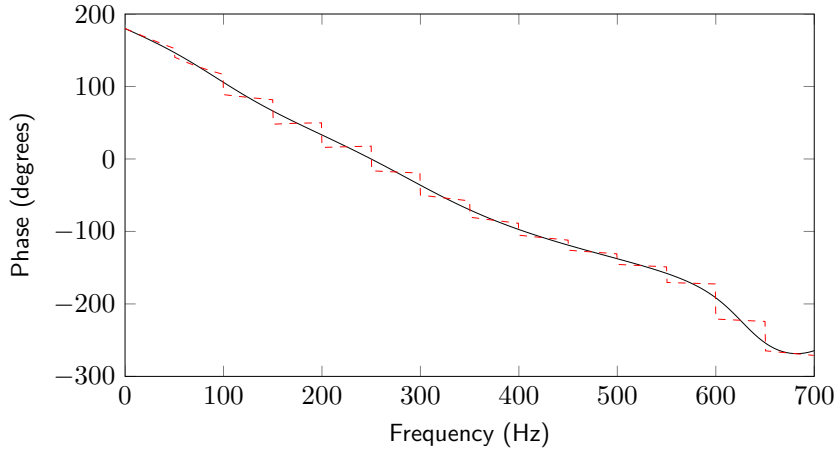

(b) Phase response.

Figure 4.3: Identification comparison between $S(z)$ (black solid line) and $\hat{S}_k(z)$ (red dashed line) when only one excitation sinusoid is employed in each frequency bin.

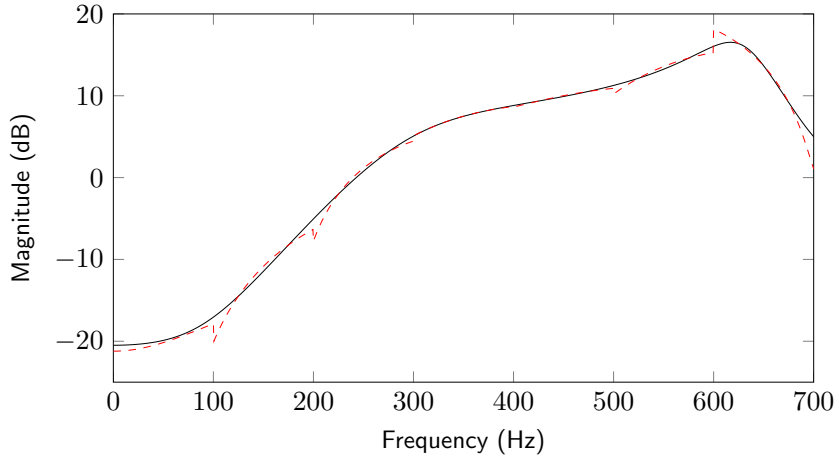

(a) Magnitude response.

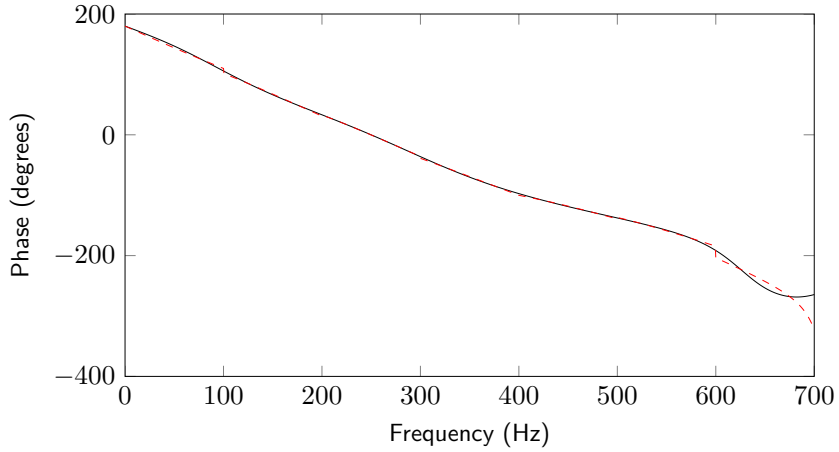

(b) Phase response.

Figure 4.4: Identification comparison between $S(z)$ (black solid line) and $\hat{S}_k(z)$ (red dashed line) when two excitation sinusoids are employed in each frequency bin.

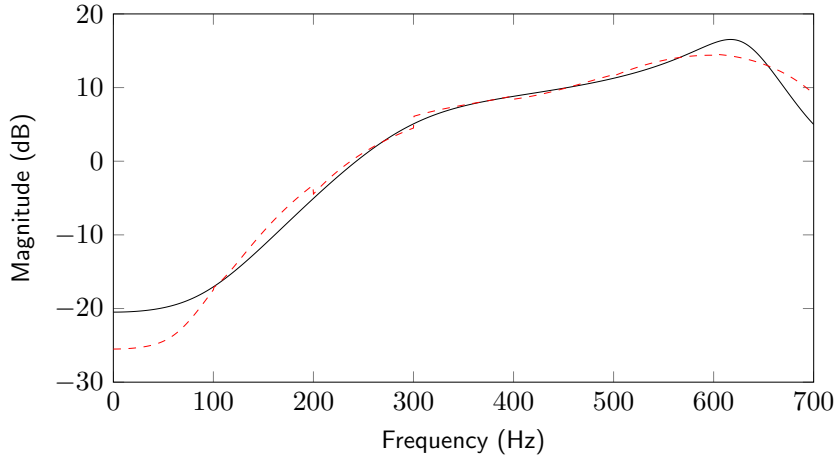

(a) Magnitude response.

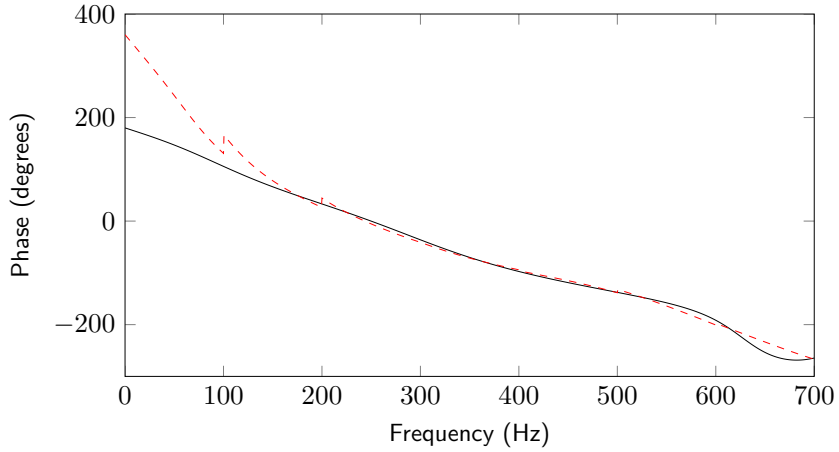

(b) Phase response.

Figure 4.5: Identification comparison between $S(z)$ (black solid line) and $\hat{S}_k(z)$ (red dashed line) when a bandpassed white-noise signal is employed in each frequency bin.

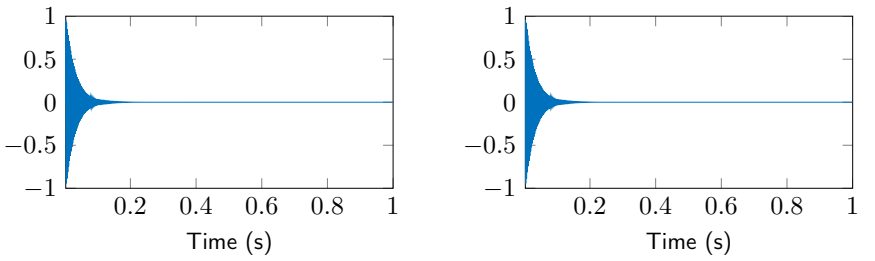

(a) Global estimate.

(b) Single-sinusoid approach.

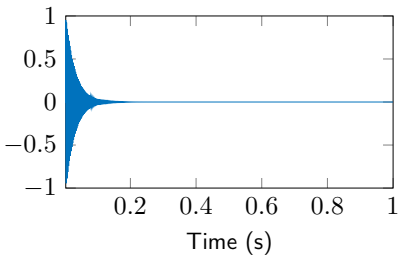

(c) Two-sinusoid approach.

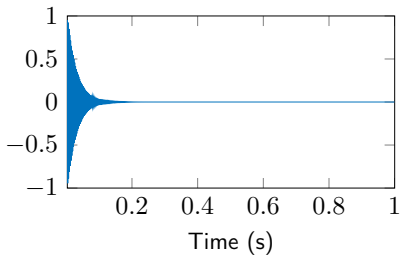

(d) Bandpassed white-noise approach.

Figure 4.6: Performance comparison between local estimation approaches. The plots show the error signal $e(n)$ when a single sinusoid at $400Hz$ must be removed.

set to $\mu_0 = 0.0011$. All the systems remove the noise after $0.2s$ without any noticeable difference. Therefore in the following simulations we will employ the single-sinusoid approach because its estimation inaccuracy does not degrade the performance of the system appreciably and it allows the lowest order for the local paths.

4.1.4 Speed of convergence and noise cancellation

In the following, computer simulations are carried out to evaluate and compare the convergence time of the proposed system with respect to the traditional ANC system, Ziegler's system and Xiao's system.

The local models $\hat{S}_k(z)$ and the global model $\hat{S}(z)$ are learnt before the operations of the system using the LMS algorithm. The order of the global model is set to $L' = 150$. The width of the frequency bins is set to $\Delta f = 50Hz$ which is small enough to ensure the 90° stability condition for all the local paths. The total number of frequency bins is $K = 14$ and the order of each local secondary path is $L = 5$. The local secondary

paths are learnt with a single sinusoidal signal at the central frequency of each frequency bin. Figure 4.2 shows a comparison between the frequency response of the local models and the actual secondary path.

In the following simulations, the secondary path $S(z)$ does not change and the online-modelling subsystem is turned off.

4.1.4.1 Simulation one: single-frequency noise

In the first simulation, $d(n)$ contains a single sinusoidal component at frequency $f_0 = 400Hz$. A step size of $\mu_0 = 0.0012$ is used to adapt the coefficients $w_0(n)$ and $w_1(n)$. The pole-attraction factor in the bandpass filter of Xiao's system is set to $\rho = 0.985$.

The convergence trajectory of the two adaptive coefficients $w_0(n)$ and $w_1(n)$ and the residual error $e(n)$ are shown in Figure 4.7. The traditional system, Xiao's system and the proposed system converge to the optimal solution in about $100ms$, whereas Ziegler's system takes roughly $200ms$.

The controlled frequency f_0 lies between two central frequencies $f_8 = 375Hz$ and $f_9 = 425Hz$ and both $\hat{S}_8(z)$ and $\hat{S}_9(z)$ yield a 10° phase-estimation error at that frequency (Figure 4.2). Despite this, the proposed system does not show any noticeable reduction in convergence time with respect to the traditional system.

The largest phase-estimation error yielded by the local secondary paths is a 30° error at frequency $f_0 = 600Hz$. We test our system in this unfavourable situation in Figure 4.8. The step size is set to $\mu_0 = 0.00024$ in both simulations. Even in this unfortunate case the proposed system exhibits roughly the same convergence time as the traditional system.

4.1.4.2 Simulation two: multiple-frequency noise

In the second simulation, $d(n)$ contains $M = 20$ sinusoids whose fundamental is $f_0 = 30Hz$ and $f_i = (i+1)f_0, i = 0, 1, \ldots 19$. The step sizes are the same in all simulations. Figure 4.9 shows the convergence of the two adaptive coefficients $w_{0,0}(n)$ and $w_{1,0}(n)$ associated to the fundamental frequency and the error signal.

The proposed system takes slightly longer than the traditional system to

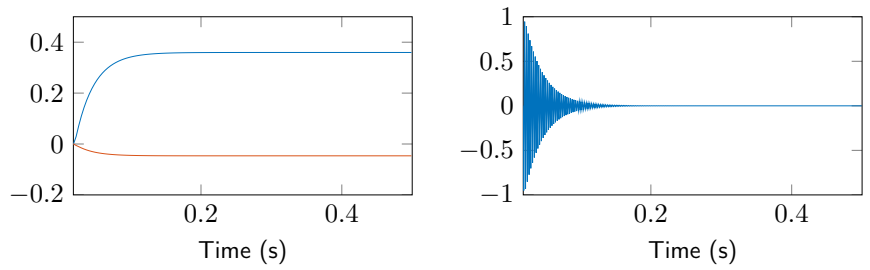

(a) Traditional system.

(b) Traditional system.

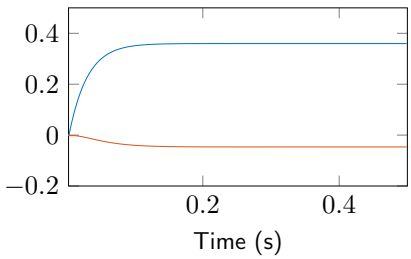

(c) Proposed system.

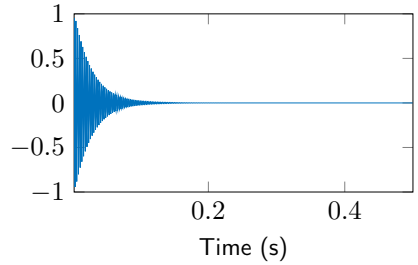

(d) Proposed system.

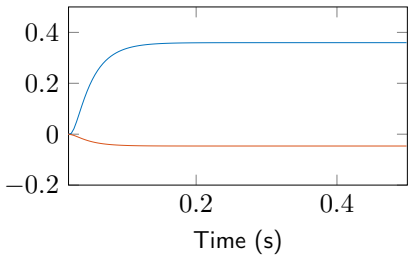

(e) Xiao's system.

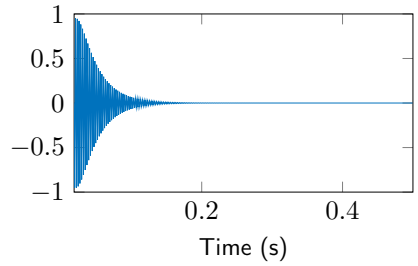

(f) Xiao's system.

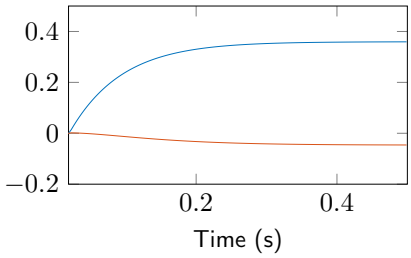

(g) Ziegler's system.

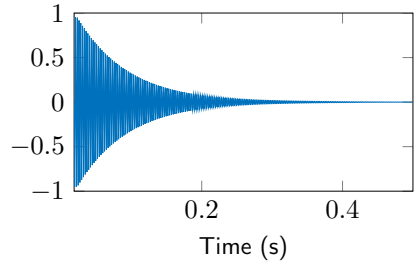

(h) Ziegler's system.

Figure 4.7: The two adaptive coefficients (on the left) and the error signal $e(n)$ (on the right) in the evaluated systems when a single frequency ($f_0 = 400Hz$) is controlled.

completely remove all the harmonics. As discussed in the previous chapters, both systems suffer from a performance degradation with respect to the

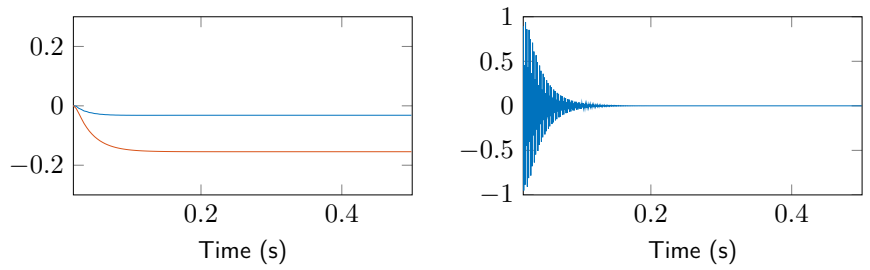

(a) Traditional system. *(b) Traditional system.*

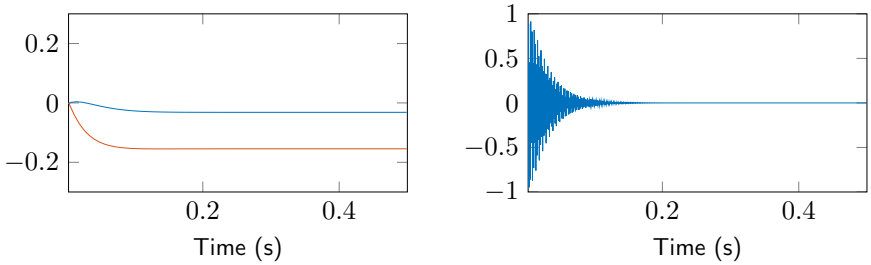

(c) Proposed system. *(d) Proposed system.*

Figure 4.8: The two adaptive coefficients (on the left) and the error signal $e(n)$ (on the right) in the traditional and proposed systems when one single frequency ($f_0 = 600Hz$) is controlled.

single-frequency case due to the fact that each controller uses a single error signal to update its adaptive coefficients. In the multiple-frequency case, in fact, the error signal will contain all the harmonic components, which will slow down the convergence of each controller.

Xiao's system struggles to remove the noise: if $\rho = 0.985$, the system is unstable because the bandwidth of the bandpass filters is not sharp enough to separate the filtered reference signals; if $\rho = 0.999$, the system is stable, but it takes longer to remove the noise with respect to the proposed and traditional systems due to the long time constant associated to the bandpass filters.

Ziegler's system is considerably slower than all three systems: after one second it is still converging to its optimal solution, as evident in the spikes of the convergence trajectory of the first couple of adaptive coefficients.

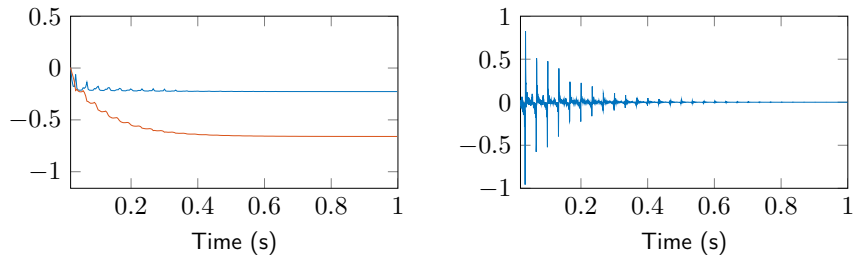

(a) Traditional system.

(b) Traditional system.

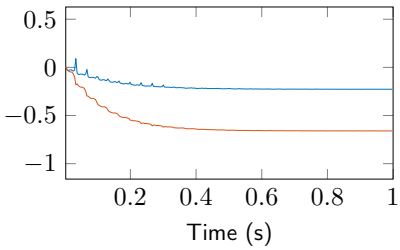

(c) Proposed system.

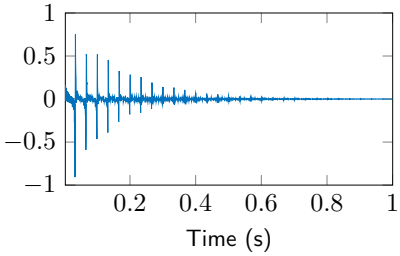

(d) Proposed system.

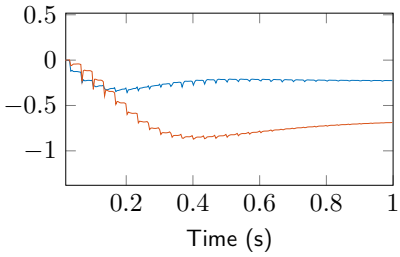

(e) Xiao's system ($\rho = 0.999$).

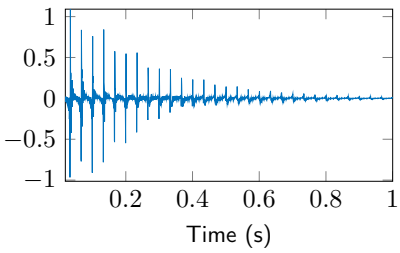

(f) Xiao's system ($\rho = 0.999$).

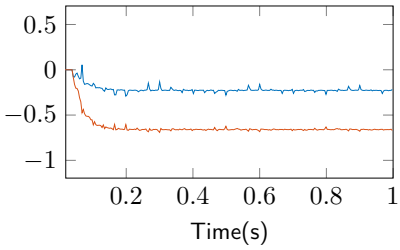

(g) Ziegler's system.

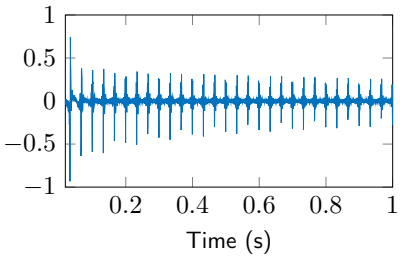

(h) Ziegler's system.

Figure 4.9: The evaluated systems when the primary signal contains a mixture of $M = 20$ sinusoids. The pictures show the adaptive coefficients associated to $f_0 = 30Hz$ on the left and the error signal $e(n)$ on the right.

4.1.4.3 Simulation three: two close frequencies

In the third simulation, $d(n)$ contains two close frequencies $f_0 = 400Hz$ and $f_1 = 401Hz$ and the step sizes are $\mu_0 = \mu_1 = 0.0012$. Figure 4.10 shows the

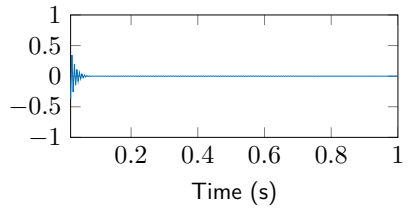

(a) Traditional system.

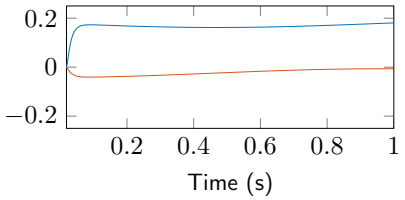

(b) Traditional system.

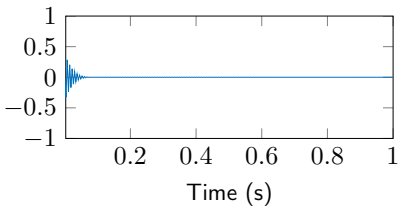

(c) Proposed system.

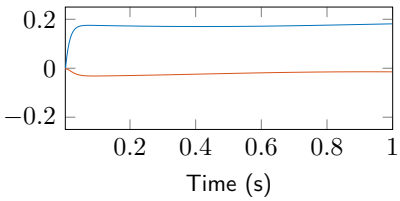

(d) Proposed system.

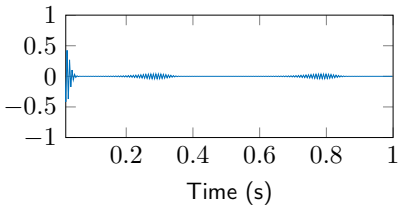

(e) Xiao's system ($\rho = 0.985$).

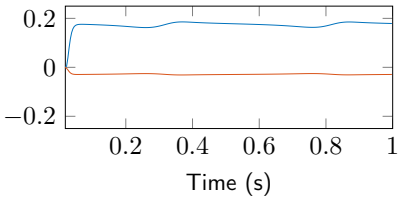

(f) Xiao's system ($\rho = 0.985$).

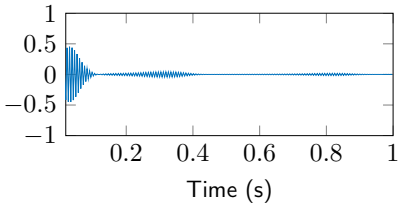

(g) Xiao's system ($\rho = 0.999$).

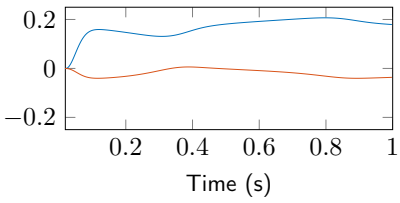

(h) Xiao's system ($\rho = 0.999$).

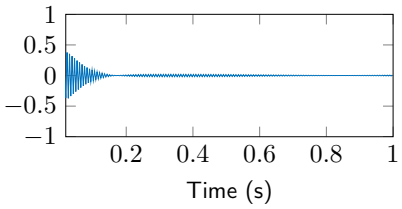

(i) Ziegler's system.

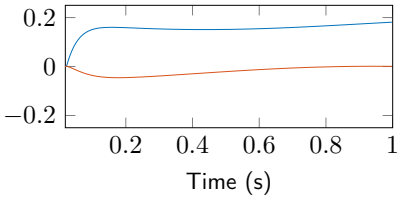

(j) Ziegler's system.

Figure 4.10: The evaluated systems when the primary signal contains two close sinusoids. On the left the error signal $e(n)$ is shown, while on the right the adaptive coefficients associated to $f_0 = 400Hz$ are shown.

adaptive coefficients $w_{0,0}(n)$ and $w_{1,0}(n)$ associated to f_0 and the residual error $e(n)$.

The proposed system and the traditional system exhibit similar performances, quickly removing the noise except for a small low-level residual.

As previously, depending on the choice of the bandwidth-control parameter ρ, Xiao's system exhibits different behaviours: if $\rho = 0.985$, the system has an oscillating behaviour with partial instabilities. If $\rho = 0.999$, the oscillating behaviour is still present but after some time the system attenuates the noise like the traditional system.

Ziegler's system exhibits an oscillating behaviour as well. The noise is reduced quickly except for an oscillating residual which is dampened after about $5s$.

4.1.4.4 Simulation four: frequency mismatch

In the fourth simulation (Figure 4.11), $d(n)$ contains one single frequency $f_0 = 300Hz$ and the step size is set to $\mu_0 = 0.0022$. The controller injects sinusoidal reference signals at the frequency $f_0^{ref} = 303Hz$, which results in a 1% frequency mismatch. Figure 4.11 shows the spectral power of the residual noise $e(n)$.

The proposed system attenuates the noise by $5dB$, which is the same noise attenuation allowed by the traditional system. This is in accordance with the theory, since narrowband ANC systems only exhibit a perfect notch at the controlled frequency (see Chapter 2).

Xiao's system exhibits an oscillating behaviour that amplifies the noise by $9dB$ during its first oscillation and converges to a $3dB$ amplification when ρ is large, while it attenuates the noise by $5dB$ when ρ is small.

Ziegler's system attenuates the noise by $2.5dB$, due to its inaccurate secondary path compensation.

4.1.4.5 Simulation five: time-varying frequency

In the fifth simulation (Figure 4.12), $d(n)$ contains one single time-varying frequency that varies linearly from $525Hz$ to $535Hz$ in $500ms$. The step size is set to $\mu_0 = 0.0004$. The frequency of the reference signal is equal to

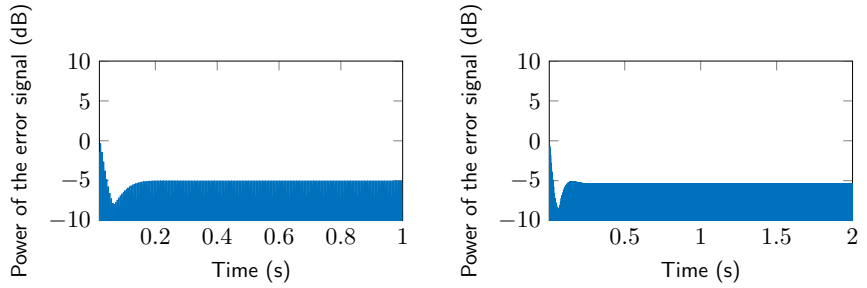

(a) Traditional system.

(b) Proposed system.

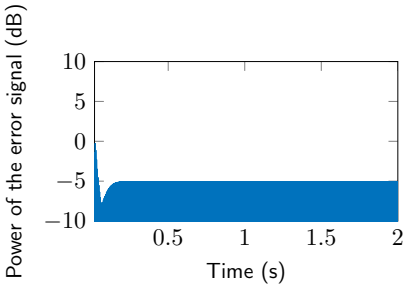

(c) Xiao's system ($\rho = 0.9$).

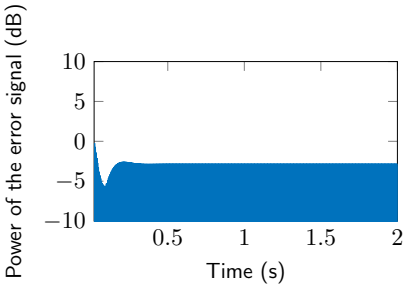

(d) Ziegler's system.

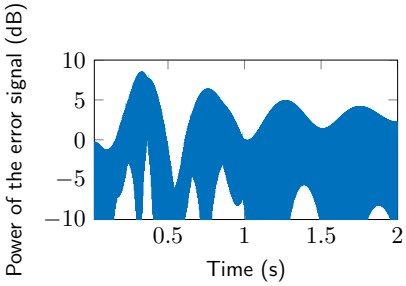

(e) Xiao's system ($\rho = 0.9995$).

Figure 4.11: The evaluated systems in the presence of 1% frequency mismatch. The pictures show the power of the error signal.

the controlled frequency at each iteration so that no frequency mismatch is present. The phase lag Δ of Ziegler's system is changed at every iteration so that its delay compensation is as accurate as possible.

The proposed system attenuates the time-varying frequency similarly to the traditional system. The systems attenuate the noise by roughly $15dB$ after $200ms$, but then the attenuation degrades by the time the linear frequency sweep is finished.

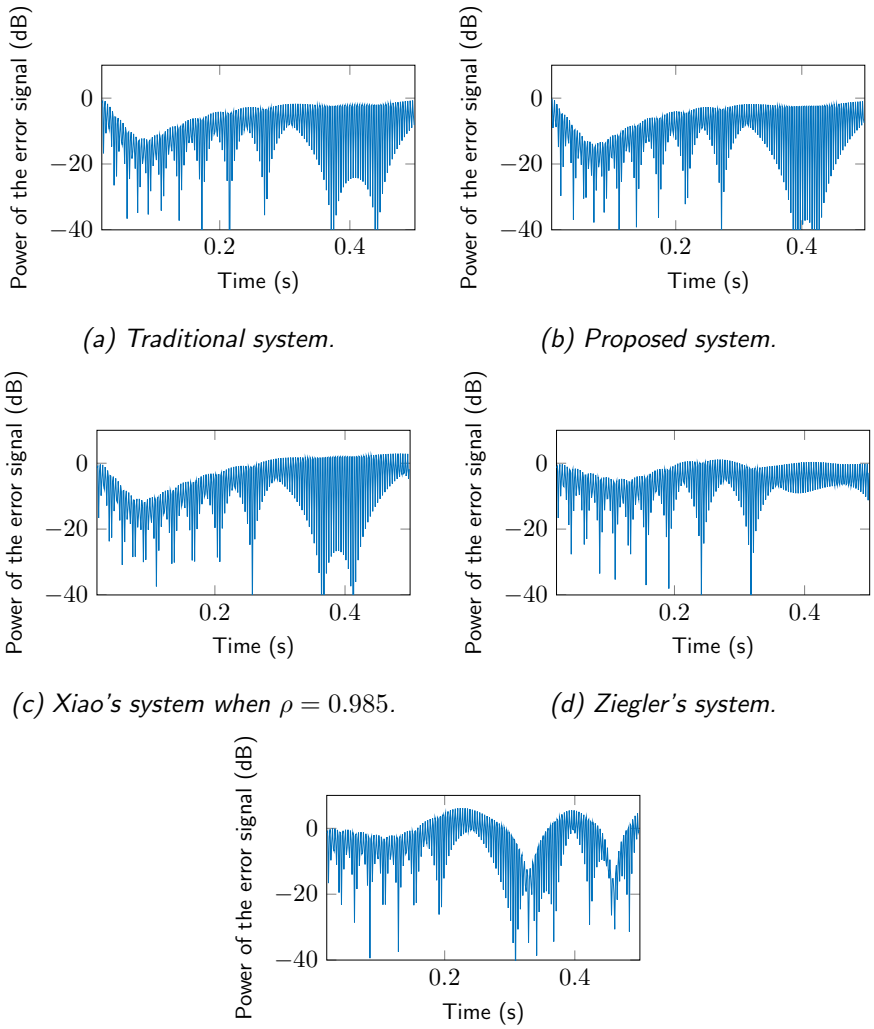

(a) Traditional system.

(b) Proposed system.

(c) Xiao's system when $\rho = 0.985$.

(d) Ziegler's system.

(e) Xiao's system when $\rho = 0.9995$.

Figure 4.12: The evaluated systems when one single time-varying frequency is controlled. The frequency varies from $525Hz$ *to* $535Hz$ *in* $500ms$*. The pictures show the power of the error signal.*

The behaviour of Xiao's system is again dependent on the choice of ρ. A small ρ yields the same performance as the proposed system and the traditional system, but a large ρ results in an oscillating behaviour during the frequency sweep.

The maximum attenuation achieved by Ziegler's system is only $5dB$ and the system amplifies the noise by $2dB$ in the middle of the frequency sweep.

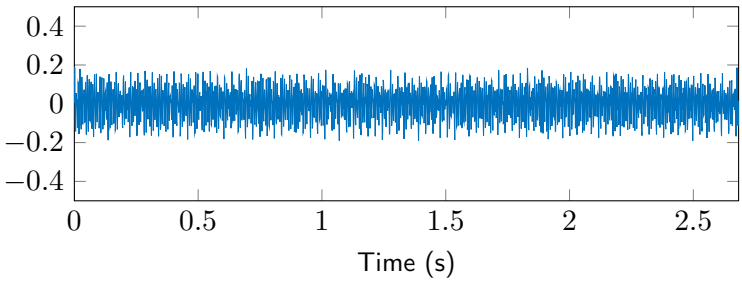

(a) The plot of the motorbike signal.

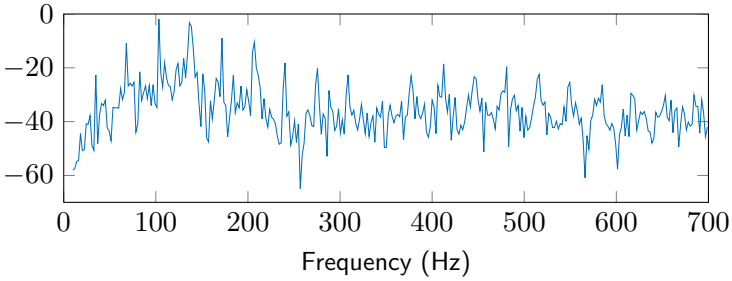

(b) The frequency spectrum of the motorbike signal.

Figure 4.13: Motorbike noise.

4.1.4.6 Simulation six: real noise

In the sixth simulation (Figure 4.14), the systems are tested against the recording of a motorbike noise, which contains a mixture of low-level broadband noise and several flickering harmonics with fundamental $f_0 = 34.26Hz$. The fundamental was estimated with the autocorrelation method. Figure 4.13 shows the plot of the motorbike noise signal and its spectrum.

The step sizes for each controlled frequency are chosen according to the empirical step size-correction law presented in the previous chapter. The average magnitude of the secondary-path model is computed in a neighbourhood of each controlled harmonic and the step sizes are chosen according to the following law:

$$\mu_i = \frac{\alpha}{A_i^{\beta}} \qquad i = 0, \ \ldots, \ M-1, \tag{4.2}$$

where A_i is the average magnitude of $\hat{S}(z)$ (or $\hat{S}_k(z)$ in the proposed system) around the controlled frequency f_i.

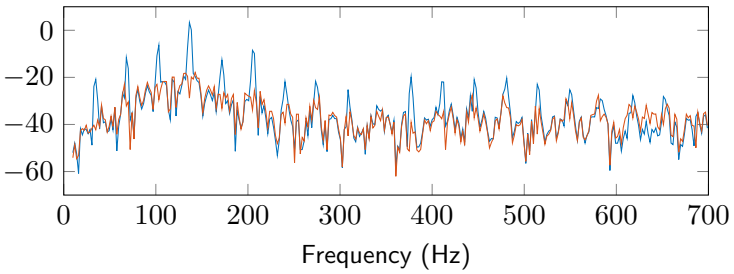

(a) Traditional system.

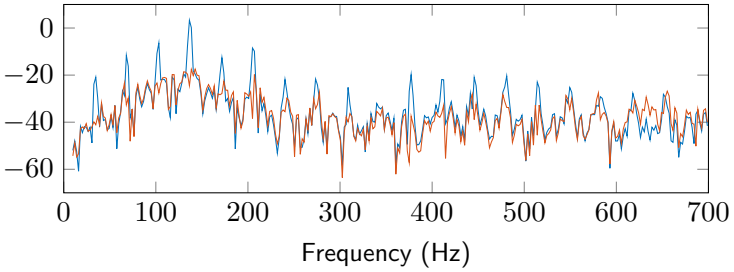

(b) Proposed system.

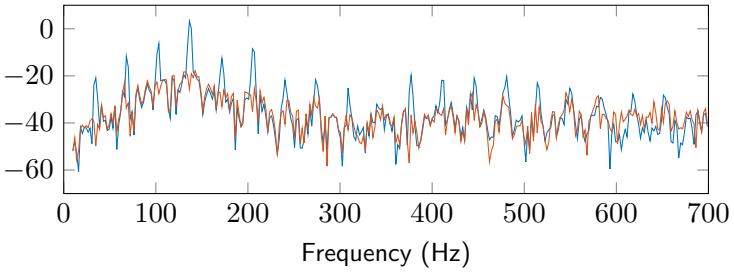

(c) Xiao's system.

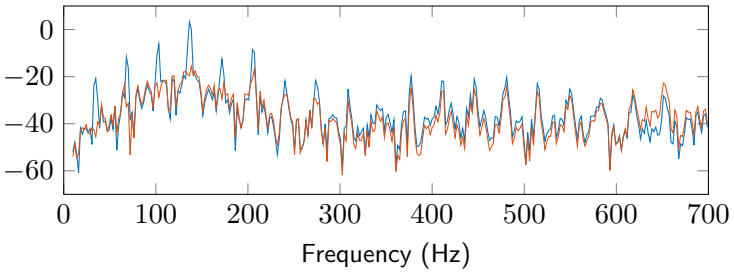

(d) Ziegler's system.

Figure 4.14: The evaluated systems when the primary signal contains motorbike noise. The pictures show the power spectral density (PSD) of the primary noise in blue and the PSD of the residual error in orange.

We set $\alpha = 0.003$ and $\beta = 2$ in the traditional system, in the proposed system and in Xiao's systems. Ziegler's system required $\alpha = 0.0005$ and $\beta = 2$ to be stable.

The traditional system removes the strongest low-frequency harmonics completely, but only attenuates the high-frequency harmonics because they fluctuate and the adaptive filter cannot track them fast enough even with a large step size. Consequently, the noise appears to be amplified between $600Hz$ and $700Hz$ because the adaptive controllers working in that range inject noise at the wrong frequency.

The proposed system removes the low-frequency harmonics completely and slightly attenuates the high-frequency harmonics as well.

Xiao's system is unstable for $\rho = 0.985$, but it achieves good noise attenuation when $\rho = 0.9995$.

Ziegler's system removes the first five low-frequency harmonics completely, but due to the lower step size needed to ensure its stability it fails to attenuate the high-frequency harmonics by more than a few dB.

4.1.4.7 Conclusions

From these simulations we can conclude that:

- Despite the inaccuracies in the phase and magnitude estimation of the local secondary paths, the proposed system offers comparable performance as the traditional system that uses a global and accurate model in terms of convergence speed and noise cancellation. This suggests that the local secondary paths may be employed in other modifications of the narrowband ANC systems to reduce the computational cost associated to global secondary-path models.

- Xiao's system has also comparable performance to the traditional system, but it relies on the proper choice of the bandwidth-control parameter ρ when the controlled frequencies are close or when multiple harmonics are being controlled: a large value for ρ determines a sharper bandwidth at the cost of a longer convergence time, while a small value for ρ determines faster convergence but it may make the system unstable since it will not separate close frequencies effectively.

	Traditional	Ziegler	Xiao	Proposed
Computational cost	High	Very low	Low	Low
Performance	High	Medium-low	Medium	Medium-high

Table 4.3: Comparison between the cost and performance of the evaluated systems.

- Ziegler's system offers the lowest computational cost of the evaluated systems, but its performance is worse than the other systems due to the inaccuracy of its delay compensation.

Table 4.3 illustrates the comparison between the evaluated systems.

4.2 Online modelling

In this section, we test the online-modelling subsystems when a global model is estimated and when several local models are estimated.

4.2.1 Problem definition

The secondary path $S(z)$ changes as shown in Figure 4.15. The change is obtained by rotating two complex-conjugate poles of $S(z)$ by 2.25° (which corresponds to a change in the resonant frequency of $50Hz$) and scaling them by a 0.88 factor. Since online modelling algorithms are not robust against abrupt step-like changes in the secondary-path transfer function, we simulate a smooth transition between the two functions as follows. If the secondary path can be written as

$$S(z) = \frac{\sum_{i=0}^{P} b_i z^{-i}}{\sum_{j=0}^{Q} a_j z^{-j}} = \frac{\mathbf{b}^T \mathbf{z_b}}{\mathbf{a}^T \mathbf{z_a}}, \tag{4.3}$$

where

- $\mathbf{b} = [b_0 \ b_1 \ \dots \ b_P]^T$ are the coefficients of the transfer function's numerator,
- $\mathbf{a} = [a_0 \ a_1 \ \dots \ a_Q]^T$ are the coefficients of the transfer function's denominator,

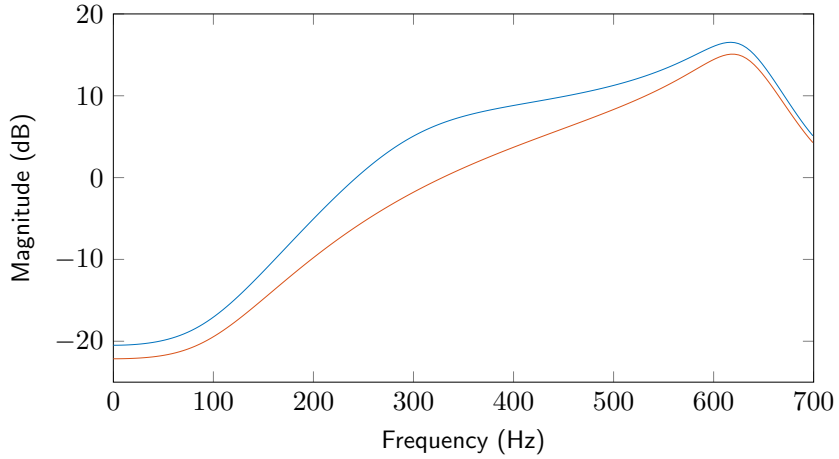

(a) Magnitude response.

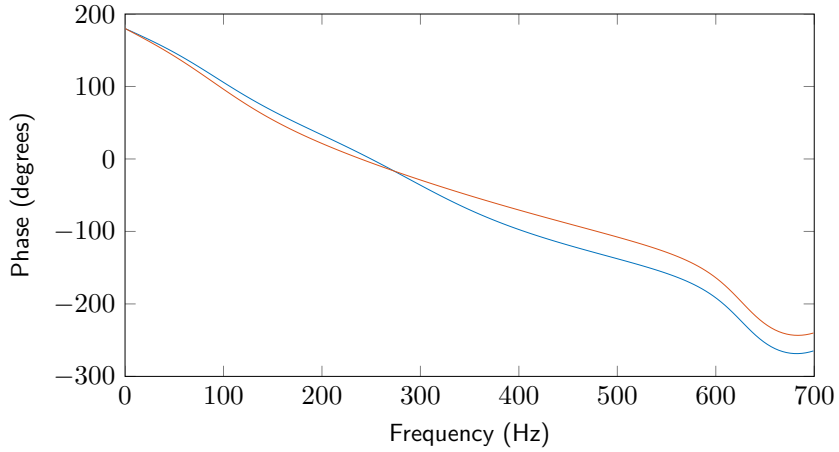

(b) Phase response.

Figure 4.15: The variation of the secondary path. The blue line represents $S(z)$ before the change, the orange one represents $S(z)$ after the change.

- $\mathbf{z_b} = [1\ z^{-1}\ \ldots\ z^{-P}]^T$ and
- $\mathbf{z_a} = [1\ z^{-1}\ \ldots\ z^{-Q}]^T$,

then the secondary-path variation follows the following law:

$$\mathbf{a}(n+1) = \alpha_a \mathbf{a}(n) + (1-\alpha_a)\mathbf{a}^{new} \tag{4.4}$$

where $\mathbf{a}^{new}$ is the denominator of the secondary path after the change. The change is triggered in the simulation at a given time and α_a controls the speed of the variation. We chose $\alpha_a = 0.985$, which means that the secondary path completes its variation in about $50ms$ (given our choice for the sampling frequency $F_s = 8000Hz$). This change is fast enough to study how the two evaluated online-modelling systems adjust to it, but not so abrupt as to determine instability.

4.2.2 Simulation seven: online modelling of a global estimate

In the seventh simulation, the online-modelling parameters are set as follows: the variance of the white-noise excitation signal is $\sigma_a^2 = 0.01$ and the normalised online-modelling step size is set to $\mu_s = 0.01$. The online-modelling subsystem uses the normalised FxLMS algorithm. The order of the global estimate $\hat{S}(z)$ is $L' = 150$. Only one ANC controller is working to remove a single frequency at $f_0 = 500Hz$.

Figure 4.16 shows the tracking capabilities of the online-modelling subsystem when the change takes place. The system is initialised with an accurate global model at time 0. After the change, the system takes about $5s$ to adjust the global model $\hat{S}(z)$ to the new secondary path $S(z)$.

4.2.3 Simulation eight: online modelling of local estimates

In the eighth simulation, the online-modelling parameters are set as follows: the normalised online-modelling step size is set to $\mu_s = 0.01$ and the amplitude of the sinusoidal excitation signals is $\overline{\delta} = 0.04$ so that the power of the overall excitation signal that is fed to the loudspeaker is the same as in the previous simulation. The online-modelling subsystem uses the normalised FxLMS algorithm. The order of the local estimates is $L = 5$ and the width

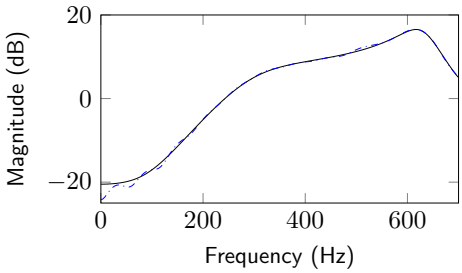

(a) Before the change.

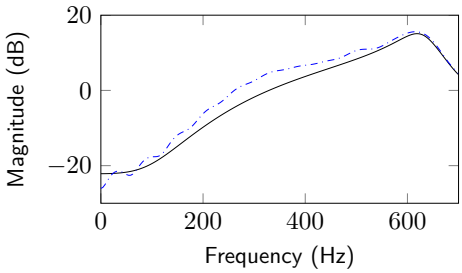

(b) 1s after the change.

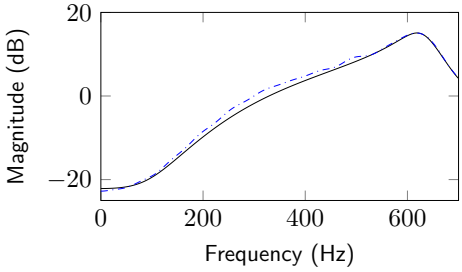

(c) 3s after the change.

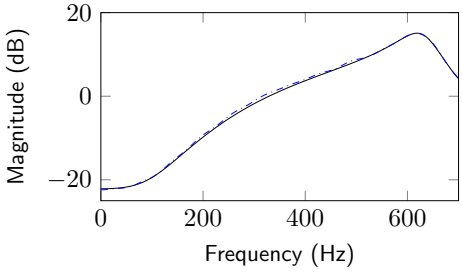

(d) 5s after the change.

Figure 4.16: Online modelling of a global secondary path. Each picture represents a snapshot of the magnitude response of $S(z,n)$ (solid line) and $\hat{S}(z,n)$ (dash-dotted line) at a given time after $S(z,n)$ changes.

of the frequency bins is $\Delta f = 50Hz$. Only one ANC controller is working to remove a single frequency at $f_0 = 500Hz$.

Figure 4.17 shows the tracking capabilities of the online-modelling subsystem when the change takes place. The system is initialised with an accurate global model at time 0. After the change, the majority of the local secondary paths converge to the new optimal solution in $600ms$. Only two local models, namely $\hat{S}_3(z)$ and $\hat{S}_4(z)$, take roughly $3s$ to converge to the new solution.

4.2.3.1 Online modelling of local estimates (two sinusoidal excitation signals)

We present here the performance of the online-modelling system when the local secondary paths are learnt with two sinusoidal excitation signals for each frequency bin. The online-modelling parameters are set as follows: the normalised online-modelling step size is set to $\mu_s = 0.01$ and the amplitude of the sinusoidal excitation signals is $\overline{\delta} = 0.04$ so that the power of the overall excitation signal that is fed to the loudspeaker is the same as in the previous simulations. The online-modelling subsystem uses the normalised FxLMS algorithm. The order of the local estimates is $L = 30$ and the width of the frequency bins is $\Delta f = 100Hz$. Only one ANC controller is working to remove a single frequency at $f_0 = 500Hz$.

Figure 4.18 shows the tracking capabilities of the online-modelling subsystem when the change takes place. The system is initialised with an accurate global model at time 0. After the change, the local secondary paths converge to the new secondary path after $4s$. As expected, this approach is slower than the single-sinusoid approach because the order of the local models is higher.

4.2.4 Computational analysis

We provide here a computational comparison between the two online-modelling systems.

The online-modelling system in the global case performs L' multiplications per iteration in order to convolve the white-noise excitation signal with

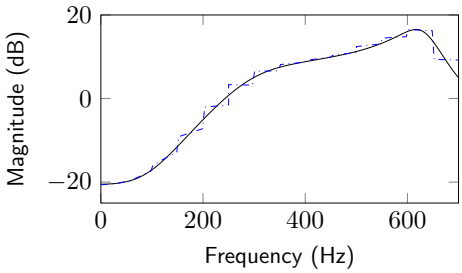

(a) Before the change.

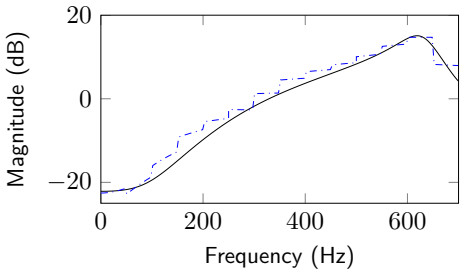

(b) 0.2s after the change.

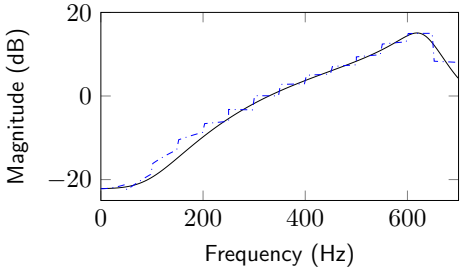

(c) 0.6s after the change.

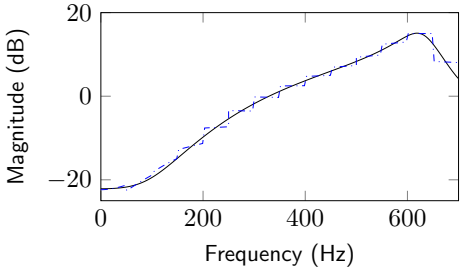

(d) 3.2s after the change.

Figure 4.17: Online modelling of $K = 14$ local secondary paths. Each picture represents a snapshot of the magnitude response of $S(z, n)$ (solid line) and $\hat{S}_k(z, n)$ (dash-dotted line) at a given time after $S(z, n)$ starts to change.

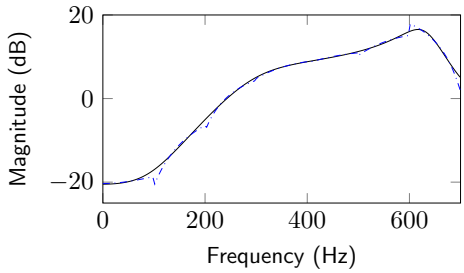

(a) Before the change.

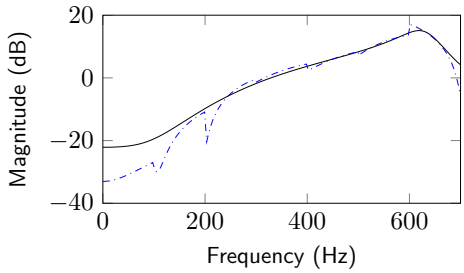

(b) 0.2s after the change.

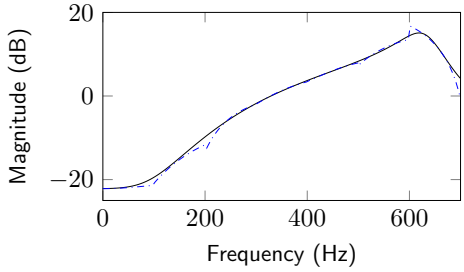

(c) 1s after the change.

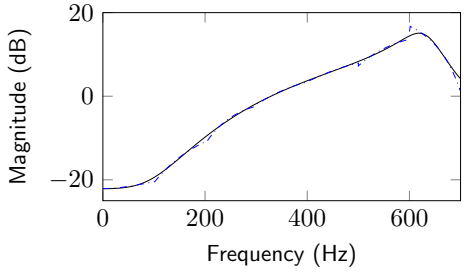

(d) 4s after the change.

Figure 4.18: Online modelling of $K = 7$ local secondary paths. Each picture represents a snapshot of the magnitude response of $S(z, n)$ (solid line) and $\hat{S}_k(z, n)$ (dash-dotted line) at a given time after $S(z, n)$ starts to change.

K \ L	2	5	10
7	14	35	70
14	28	70	140
21	42	105	210

Table 4.4: The number of multiplications per iteration performed by the proposed online-modelling system as a function of the order of the local estimates L and the number of frequency bins K.

the current global estimate. In the local case the number of performed multiplications depends on the order of the local estimates L and the number of frequency bins K (Table 4.4). In the simulations we performed, L' must be at least 100 to yield a decent spectral approximation of the secondary path, whereas $K = 14$ local estimates of order $L = 2$ are enough to ensure that the phase-estimation error stays well below the 90° stability condition. In this case, the proposed system performs only $KL = 28$ multiplications per iteration instead of $L' = 100$. The amount of performed multiplications can be reduced further if the system only updates the local models that are currently being used by the ANC units, instead of updating all K local models (see Chapter 3).

4.2.5 Conclusions

The simulations showed that the online modelling of local estimates is considerably more reactive to changes in the secondary path with respect to the online modelling of a global estimate, thanks to the lower order of the local models. The proposed system can be $\frac{5s}{3.2s} \approx 2$ times faster than the conventional online-modelling system in tracking the secondary path ($\frac{5s}{0.6s} \approx 8$ faster for some local secondary paths). Moreover, it requires fewer multiplications because in practice we only need to update the local models that are currently being used by the ANC units.

Chapter 5

Conclusions and future research directions

In this thesis, a novel narrowband ANC system has been proposed. The system is based on the identification of low-order secondary-path estimates (called *local secondary paths*) that reduce the computational cost associated to the reference-filtering operations in the traditional narrowband ANC system. The low order allowed by the local secondary paths determines an increase in the reactivity to changes in the secondary path, which makes the resulting system more robust to time-varying environments than systems that rely on a global high-order estimate of the secondary path. An empirical step size-correction law is also proposed to automatically tune the step size of each controller in parallel-form narrowband ANC systems.

Simulations show that the proposed system offers comparable performance to the traditional narrowband ANC system while reducing the cost of the reference-filtering operations by a factor of 30 and that it outperforms two other cost-effective systems in the literature in some situations. Moreover, the local online-modelling scheme is more reactive to smooth changes in the secondary path by a factor of 2 with respect to the global offline-modelling scheme and it requires fewer multiplications.

Future research directions include: a detailed theoretical performance analysis of the proposed system and its DSP-based implementation. The

cost reduction offered by the proposed system makes it a viable choice for low-energy narrowband ANC applications, such as hearing-protection headsets for industrial workers.

Bibliography

[1] B Widrow et al. Adaptive noise cancelling: Principles and applications. *Proceedings of the IEEE*, 63(12), 1975.

[2] J.C. Burgess. Active adaptive sound control in a duct: A computer simulation. *Journal of the Acoustical Society of America*, 70(1), 1981.

[3] E. Ziegler Jr. Selective active cancellation system for repetitive phenomena, 1989.

[4] Yegui Xiao. New narrowband active noise control systems requiring considerably less multiplications. In *Signal Processing Conference, 2008 16th European*, 2008.

[5] P. Lueg. Process of silencing sound oscillations, 1936.

[6] Sen M. Kuo and Dennis R. Morgan. *Active Noise Control Systems: Algorithms and DSP Implementations*. Wiley, 1996.

[7] Woon-Seng Gan and D.R. Morgan. Active noise control: A tutorial review. *Proceedings of the IEEE*, 87(6), 1999.

[8] L.J. Eriksson. Development of the filtered-u algorithm for active noise control. *Journal of the Acoustical Society of America*, 89(1), 1991.

[9] J.C. Burgess. Adaptive noise canceling applied to sinusoidal interferences. *IEEE Transactions on Acoustics, Speech, and Signal Processing*, 25(6), 1977.

[10] P.A. Regalia. An improved lattice-based adaptive iir notch filter. *IEEE Transactions on Signal Processing*, 39(9), 1991.

[11] C.-Y. Chang and S.M. Kuo. Complete parallel narrowband active noise control systems. *IEEE Transactions on Audio, Speech and Language Processing*, 21(9), 2013.

[12] J. Cheer and S.J. Elliott. Comments on complete parallel narrowband active noise control systems. *Audio, Speech, and Language Processing, IEEE/ACM Transactions on*, 22(5), 2014.

[13] Hyeon-Jin Jeon et al. Frequency mismatch in narrowband active noise control. In *Acoustics Speech and Signal Processing (ICASSP), 2010 IEEE International Conference on*, 2010.

[14] Y. Xiao et al. A new narrowband active noise control system in the presence of sensor error. In *Circuits and Systems, 2004. MWSCAS 04. The 2004 47th Midwest Symposium on*, 2004.

[15] Hyeon-Jin Jeon, Tae-Gyu Chang, Sungwook Yu, and Sen M. Kuo. A narrowband active noise control system with frequency corrector. *IEEE Transactions on Acoustics, Speech, and Signal Processing*, 19(4), 2011.

[16] Ruchi Kukde, M.S. Manikandan, and G. Panda. Development of a novel narrowband active noise controller in presence of sensor error. In *Advances in Computing, Communications and Informatics (ICACCI, 2014 International Conference on*, 2014.

[17] W. F. Meeker. Components characteristics for an active ear defender. *Journal of the Acoustical Society of America*, 29(1252), 1957.

[18] E. D. Simshauser and M. E. Hawley. The noise canceling headset: an active ear defender. *Journal of the Acoustical Society of America*, 27(207), 1955.

[19] Woon-Seng Gan and Sen M. Kuo. An integrated audio and active noise control headsets. *IEEE Transactions on Consumer Electronics*, 48(2), 2002.

[20] Sen M. Kuo, Sohini Mitra, and Woon-Seng Gan. Adaptive feedback active noise control headset: Implementation, evaluation and its extensions. *IEEE Transactions on Consumer Electronics*, 51(3), 2005.

[21] Sen M. Kuo, Sohini Mitra, and Woon-Seng Gan. Active noise control system for headphone applications. *IEEE Transactions on Control Systems Technology*, 14(2), 2006.

[22] Sen M. Kuo, Kevin Kuo, and Woon-Seng Gan. Active noise control: Open problems and challenges. In *Green Circuits and Systems (ICGCS), 2010 International Conference on*, 2010.

[23] Yong-Kim Chong, Liang Wang, See-Chiat Ting, and Woon-Seng Gan. Integrated headsets using the adaptive hybrid active noise control system. In *Information, Communications and Signal Processing, 2005 Fifth International Conference on*, 2005.

[24] Ying Song, Yu Gong, and Sen M. Kuo. A robust hybrid feedback active noise cancellation headset. *IEEE Transactions on Speech and Audio Processing*, 13(4), 2005.

[25] Thomas Schumacher, Hauke Krueger, Marco Jeub, Peter Vary, and Christophe Beaugeant. Active noise control in headsets: a new approach for broadband feedback anc. In *Acoustics, Speech, and Signal Processing, 2011 IEEE International Conference on*, 2011.

[26] Hideaki Sakai and Shigeyuki Miyagi. Analysis of the adaptive filter algorithm for feedback-type active noise control. In *Acoustics, Speech, and Signal Processing, 2001 IEEE International Conference on*, 2001.

[27] Jian Liu, Jinwei Sun, Yegui Xiao, and Lin Sun. Dynamic properties of feedback active noise control with sinusoidal primary noise. In *Mechatronics and Automation (ICMA), 2010 International Conference on*, 2010.

[28] Seong-Pil Moon, Jeong Woo Lee, and Tae-Gyu Chang. Performance analysis of an adaptive feedback active noise control based earmuffs system. *Applied Acoustics*, 96(1), 2015.

[29] Cheng-Yuan Chang and Sheng-Ting Li. Active noise control in headsets by using a low-cost microcontroller. *IEEE Transactions on Industrial Electronics*, 58(5), 2011.

[30] Say-Wei Foo, T.N. Senthilkumar, and Charles Averty. Active noise cancellation headset. In *Circuits and Systems, 2005. ISCAS 2005. IEEE International Symposium on*, 2005.

[31] Woon-Seng Gan and Sen M. Kuo. Integrated active noise control communication headsets. In *Circuits and Systems, 2003. ISCAS '03. Proceedings of the 2003 International Symposium on*, 2003.

[32] Jiun-Hung Lin, Shih-Tsang Tang, et al. Evaluation of speech intelligibility for feedback adaptive active noise cancellation headset. In *Biomedical and Pharmaceutical Engineering, 2006. ICBPE 2006. International Conference on*, 2006.

[33] Markus Guldenschuh. Secondary-path models in adaptive-noise-control headphones. In *Systems and Control (ICSC), 2013 3rd International Conference on*, 2013.

[34] Markus Guldenschuh and Robert Hoeldrich. Prediction filter design for active noise cancellation headphones. *IET Signal Processing*, 7(6), 2013.

[35] Nobuhiro Miyazaki, Kohei Yamakawa, and Yoshinobu Kajikawa. Head-mounted active noise control system to achieve speech communication. In *Signal and Information Processing Association Annual Summit and Conference (APSIPA), 2013 Asia-Pacific*, 2013.

[36] Kishan P. Raghunathan, Sen M. Kuo, and Woon-Seng Gan. Active noise control for motorcycle helmets. In *Green Circuits and Systems (ICGCS), 2010 International Conference on*, 2010.

[37] J.-H. Lin, P.-C Li, S.-T. Tang, P.-T. Liu, and Young S.-T. Industrial wideband noise reduction for hearing aids using a headset with adaptive-feedback active noise cancellation. *Medical and Biological Engineering and Computing*, 43(6), 2005.

[38] Boaz Rafaely. Active noise reducing headset: an overview. In *The 2001 International Congress and Exhibition on Noise Control Engineering*, 2001.

[39] Yoshinobu Kajikawa, Woon-Seng Gan, and Sen M. Kuo. Recent applications and challenges on active noise control. In *Image and Signal Processing and Analysis (ISPA), 2013 8th International Symposium on*, 2013.

[40] Ben Rudzyn and Michael Fisher. Performance of personal active noise reduction devices. *Applied Acoustics*, 96(1), 2012.

[41] E. A. G. Shaw and G. J. Thiessen. Acoustics of circumaural earphones. *Journal of the Acoustical Society of America*, 34(9), 1962.